https://doi.org/10.5194/egusphere-2022-1371
Preprint. Discussion started: 15 December 2022

Assimilation sensitivity of satellite-derived surface melt into the Regional Climate Model MAR: case study over the Antarctic Peninsula

Thomas Dethinne[1,2], Quentin Glaude[1,2], Ghislain Picard[3], Christoph Kittel[4], Anne Orban[2], and Xavier Fettweis[1]

[1]University of Liège, Laboratory of Climatology, Liège, Belgium
[2]University of Liège, Centre Spatial de Liège, Laboratory of Signal Processing, Liège, Belgium
[3]Institut des Géosciences de l'Environnement (IGE), Université Grenoble Alpes/CNRS/UMR 5001, Grenoble, France
[4]Institut des Géosciences de l'Environnement (IGE), Université Grenoble Alpes/CNRS/IRD/G-INP, Grenoble, France

Correspondence: Thomas Dethinne (tdethinne@uliege.be)

Abstract. The study of the recent variability and the future projections of the poles' climate currently relies on polar-oriented Regional Climate Models (RCMs). However, RCMs are subject to biases and systematic errors that impact the results of their simulations. Remote Sensing (RS) data can help to reduce these ambiguities by providing indirect observations to the modeled estimates. Using the behavior of radiofrequency signals with regard to the presence of water in a snowpack, passive and active microwave instruments such as AMSR2, ASCAT, and Sentinel-1 are used to detect melt at the surface of the snowpack. In this paper, we investigate the sensitivity of the RCM "Modèle Atmosphérique Régional" (MAR) to the assimilation of surface melt occurrence estimated by RS datasets. The assimilation is performed by nudging the MAR snowpack temperature to match the observed melt state by satellite. The sensitivity is tested by modifying parameters of the assimilation: (i) the depth to which MAR snowpack is warmed up or cooled down (corresponding to the penetration depth of the satellites) to match with satellite, and (ii) the quantity of water required into the snowpack to qualify a MAR pixel as melting or not, and (iii) by assimilating multiple RS datasets. The data assimilation is performed over the Antarctic Peninsula for the 2019-2021 period. The results show an increase in the melt production (+66.7 % on average, or +95 Gt) going along with a small decrease in surface mass balance (SMB) (-4.5 % on average, or -20 Gt) for the 2019-2020 melt season. The model is sensitive to the three parameters tested but with different orders of magnitude. The sensitivity to the assimilated dataset is reduced by using multiple datasets during the assimilation and discarding the remote observations that are not coherent. For the other two parameters, the penetration depth has more impact on the assimilation than the quantity of liquid water used as melt threshold. The first one is especially sensitive for the sensors with a shorter penetration depth. In the first centimeters, a densification due to a refreeze can impact the melt production and cause an overestimation of the melt production. For the second threshold, the impact is more important on the number of melt days rather than the melt production itself. The values tested for the quantity of liquid water required into the snowpack to qualify a MAR pixel as melting or not (0.1 or 0.2 % of the snowpack mass being water) are lower than during typical melt days (∼1.2 %) and impact results mainly at the beginning and end of the melt period when lower

https://doi.org/10.5194/egusphere-2022-1371
Preprint. Discussion started: 15 December 2022

values are reached. Such an assimilation will allow an uncertainty estimation of MAR's melt production, as well as identifying potential issues at the snowpack surface processes.

1 Introduction

The polar ice sheets contain more than two-thirds of the planet's freshwater (Church et al., 2013). If melted entirely, the Antarctic ice sheet (AIS) would cause an elevation of the sea level of 56 m (Fretwell et al., 2013). As for now, the AIS is mainly losing mass from basal melting and calving (The IMBIE Team, 2018; Rignot et al., 2019; Adusumilli et al., 2020). However, surface melting is becoming an increasing concern with climate change (Trusel et al., 2015; Bell et al., 2018; Gilbert and Kittel, 2021). Over the ice shelves, the floating boundaries of the ice sheet, the surface melt is known to weaken the structure of the shelf and can cause hydrofracturing, leading to even more mass loss(Scambos et al., 2003; Pollard et al., 2015; Lai et al., 2020). The thinning of the ice shelves also has consequences on the ice flow of the AIS. Although the ice shelves are smaller than the ice sheet, they exercise a buttressing effect on the upstream ice flow, controlling the quantity of ice reaching the surrounding ocean. Their thinning reduces that buttressing effect and consequently leads to an increase in mass loss (Favier and Pattyn, 2015; Paolo et al., 2015; Sun et al., 2020).

Climate models are nowadays one of the handiest tools to monitor the ice shelf evolution. For example, MAR (for "Modèle Atmosphérique Régional" in French) has been developed to monitor the polar ice sheets. However, Regional Climate Models (RCMs) still have some limitations. Because of the forcing, or the physical assumptions, the models may contain significant uncertainties. Those may be reduced by using external data with other independent sources of uncertainties to correct the model at certain points in space and/or time. This technique is known as "data assimilation" and is commonly applied in numerous fields where observations can be integrated into a model (Evensen, 2009; Bouchard et al., 2010; Navari et al., 2018; Landmann et al., 2021).

In this article, we sequentially assimilate satellite-derived surface melt occurrence over the Antarctic Peninsula (AP), West Antarctica, into the MAR model. Three major ice shelves are located over the AP: Larsen C, Georges VI, and Wilkins (Figure 1). These ice shelves undergo the most surface melt of the AIS, and their surface processes are also poorly understood, with a complex surface hydrology (Barrand et al., 2013; Datta et al., 2019; Johnson et al., 2020).

The highly uneven topography of the area is challenging for the RCMs usually operating at kilometer-scale resolution. Localized phenomena like Foehn-effect induce melt can occur at a smaller spatial extent than the RCMs spatial resolution (Datta et al., 2019; Chuter et al., 2022; Wille et al., 2022). However, high-resolution satellites can document these local events that could be missed by RMCs in case of localized or extreme events. In addition, using multiple satellites allows us to perform the assimilation over the whole studied zone every day for two melt seasons (2019-2020 and 2020-2021). As for now, assimilating remotely sensed products in RCMs is a promising method to quantify the surface meltwater quantity in Antarctica. The scarcity of field observations and the complexity of the surface hydrology (Bell et al., 2018) make it hard to evaluate and constrain models otherwise.

https://doi.org/10.5194/egusphere-2022-1371
Preprint. Discussion started: 15 December 2022

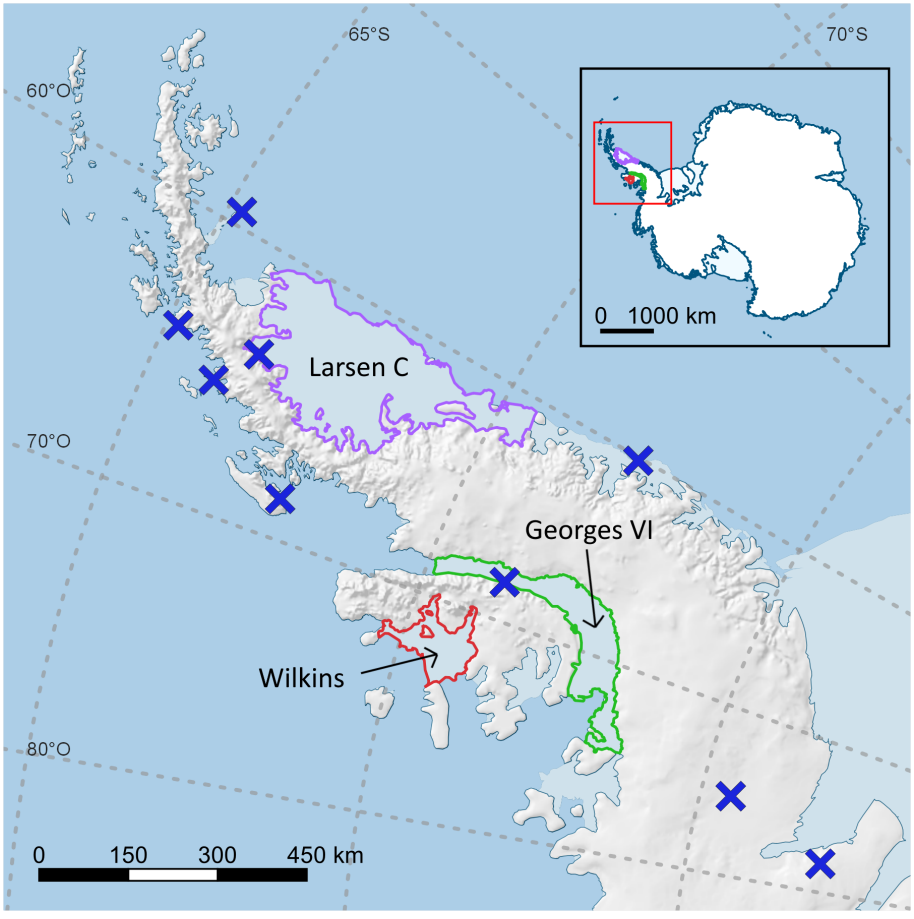

Figure 1. Location of the Antarctic Peninsula and the three studied ice shelves. The ice shelves are denoted by color outlines. Larsen C is outlined in purple, Georges VI in green, and Wilkins in red. Blue crosses indicate the position of the weather stations used for the evaluation of the model (Sect. 3).

Modeling the surface melt production on the ice shelves is important for several reasons. One consequence of surface melting is the hydrofracturing, which destabilizes the ice shelves and therefore induces high mass loss (Donat-Magnin et al., 2021). Hydrofracturing is impacted by the melting/snowfall ratio and by the snowpack capacity to retain and refreeze meltwater (Donat-Magnin et al., 2021; Gilbert and Kittel, 2021), a proper modeling of the surface melt is needed to study the conditions leading to the destabilization. In addition, proper modeling of the surface melt also makes possible the study of the evolution of the snowpack during strong melt events. Studying the snowpack ability to retain liquid water is crucial because the Antarctic snowpack could saturate, and stop absorbing surface meltwater in the future, as observed currently over the Greenland ice sheet (Noël et al., 2017).

In this work, we present the results of the assimilation of satellite-derived melt into MAR and the methodology applied to test the sensitivity of the model to the assimilation. Experiments have been performed by varying the depth to which the

https://doi.org/10.5194/egusphere-2022-1371
Preprint. Discussion started: 15 December 2022

snowpack temperature is changed (called the penetration depth here after) to match satellites, the minimum water quantity to consider the model state as melting, and the assimilated melt product.

Depending on the context of the study, like the region of interest, the length, or the resolution, the use of a specific satellite dataset over another can be useful as depending on the sensor and acquisition times, melt occurrence can be different (Husman et al., 2022). On the one hand, the passive sensors tend to have coarser resolution than the active ones and provide information with higher uncertainties in areas with complex topography. Nonetheless, they provide daily images with melt detection algorithms that have proven to be efficient (Zwally and Fiegles, 1994; Torinesi et al., 2003; Colosio et al., 2021), and have been available for a longer time in the past. On the other hand, active sensors have a better spatial resolution but may have a lower revisit time. The choice of the assimilated dataset can thus influence the results of the model.

The satellite data, the model and the assimilation are presented in Sect. 2. The validation of the model is described in Sect. 3. The results of the sensitivity tests when assimilating data into the model are discussed in Sect. 4. Finally, a general conclusion and discussions on the perspectives of the assimilation of remote sensing data in the MAR model are included in Sect. 5.

2 Methods and data

2.1 Satellite data

Three satellite datasets were used to create the binary melt masks. The three sensors operate in the microwaves (GHz spectrum). Microwave radiometers are commonly used to map snow cover, sea ice, or the extension of surface melt over ice sheets (Parkinson, 2001; Torinesi et al., 2003; Fettweis et al., 2011; Colosio et al., 2021). The signal is used to detect if the snowpack is wet or not as microwaves interact with water. The presence of liquid water in the snowpack induces a change of its emissivity and absorptivity. This change leads to a change in the satellite observables, the backscattering coefficient σ_0 for active sensors and the brightness temperature for passive sensors (Mätzler, 1987; Zwally and Fiegles, 1994; Johnson et al., 2022; Picard et al., 2022). In this study, the presence of liquid water below the surface of the snowpack is interpreted as melting.

Using microwaves also brings other advantages such as atmospheric transparency and day/night acquisition capabilities. However, the low resolution of radiometers is problematic to determine small scale melt extents (Datta et al., 2018). The surface of one pixel is observed as homogeneous. With pixels of 100 km^2 a majority of the pixels are overlapping regions with different land cover or topography (Johnson et al., 2020). To override some limitations of the passive sensors, we also employed active sensors. In this case, the active sensors have a better spatial resolution than the passive ones but longer revisit time. In total, four melt masks are created from three sensors: one radiometer, one scatterometer and a radar.

In this study, we used The Advanced Microwave Scanning Radiometer 2 (AMSR2) aboard the Global Change Observation Mission - Water "SHIZUKU" (GCOM-W1) retrieved from the Japan Aerospace Exploration Agency (JAXA) G-Portal (JAXA, 2021). Thanks to the sun-synchronous orbit at an altitude of 700 km, daily observations of the polar regions are obtained. The level-3 products contain the daily mean brightness temperature in horizontal polarization at the 18.7 GHz channel, gridded at a 10km resolution. The 18.7 GHz channel is used as it is slightly more sensitive to liquid water content than the others (Picard et al., 2022). Ascending and descending paths were processed separately to create two melt masks.

https://doi.org/10.5194/egusphere-2022-1371
Preprint. Discussion started: 15 December 2022

Melt detection is based on a change of the snowpack's physical properties. Dry, the snowpack has a lower emissivity (ϵ) than wet, changing the microwave behaviors in the snowpack (Mätzler, 1987). For the passive microwave sensors, this change is observed through an augmentation of brightness temperature (Figure 2), caused by the increase in emissivity (Zwally and Fiegles, 1994) :

$$TB(\lambda) = \epsilon * TP \tag{1}$$

with TB(λ) the wavelength-dependent brightness temperature, and TP the temperature as a physical quantity. The melt retrieval technique applied for this study is a statistical approach developed by Fahnestock et al. (2002) and modified by Johnson et al. (2020). The melt detection is performed through a K-mean clustering algorithm (Figure 3). The algorithm is applied to the annual time series of brightness temperature. Melt is assumed when the time series show a binomial distribution. Criterias and thresholds used are the same as in Johnson et al. (2020) to assume the binomial distribution.

To ensure coherency between remote sensing products and our climate model, the melt masks are interpolated on a common grid. Grids are overlapped and for each MAR pixel, the state of melting is determined by the most dominant melt/no-melt surface of the satellite mask. This interpolation is made with the hypothesis that the deformations and variations of the area caused by the spatial projection are negligible between a pixel and its neighbors.

The radar dataset is retrieved from the Sentinel-1 (S1) satellites constellation from the European Space Agency's (ESA) Copernicus space program. Starting with the launch of S1-A in 2014, the Sentinel-1 constellation gives access to data combining high spatial resolution and lower revisit time covering most of the globe. With the Synthetic Aperture Radar (SAR) technology, S1 products reach a spatial resolution of the order of tens of meters every 6 days. By combining different orbital paths, it is possible to reduce the time between two observations of the same location to 2-3 days in the AP. Working in C-band (5.405 GHz), these SAR sensors can react to the presence of liquid water in the snowpack with changes in backscattering coefficient σ_0 (Figure 4). With the increase in liquid water in the snowpack, comes a change in absorptivity and in scattering mechanism (Nagler and Rott, 2000; Johnson et al., 2020). These two phenomena both lead to a decrease in the observed backscattering coefficient σ_0 (Moreira et al., 2013). As this coefficient changes little in Antarctica as long as the snowpack is dry, it is assumed that a significant change in backscattering is likely caused by the presence of water in the snowpack.

As for the passive sensors, several algorithms have been proposed to detect water in snow with SAR and active sensors in general. Depending on the polarization, the frequency, and the nature of the snowpack, the threshold applied to the backscattering values is variable (Winebrenner et al., 1994; Koskinen et al., 1997; Nagler et al., 2016). For a C-band radar, a 3-dB decrease in σ_0 has been employed as a threshold by Nagler and Rott (2000) and Johnson et al. (2020). Later, Liang et al. (2021) proposed a -2.66 dB threshold after the normalization of the images to their winter mean as the threshold was found to be effective on the Antarctic ice sheet.

To minimize the time between two acquisitions of Sentinel-1, all the available images were processed. To handle the quantity of data, image processing was carried out on Google Earth Engine (GEE, Gorelick et al., 2017). The S1 dataset available on GEE is already preprocessed following the implementation of the Sentinel-1 Toolbox from ESA (GEE, 2022; ESA, 2022). These processing operations include an update of the orbit metadata, removal of the low-intensity noise on the scene edges,

https://doi.org/10.5194/egusphere-2022-1371
Preprint. Discussion started: 15 December 2022

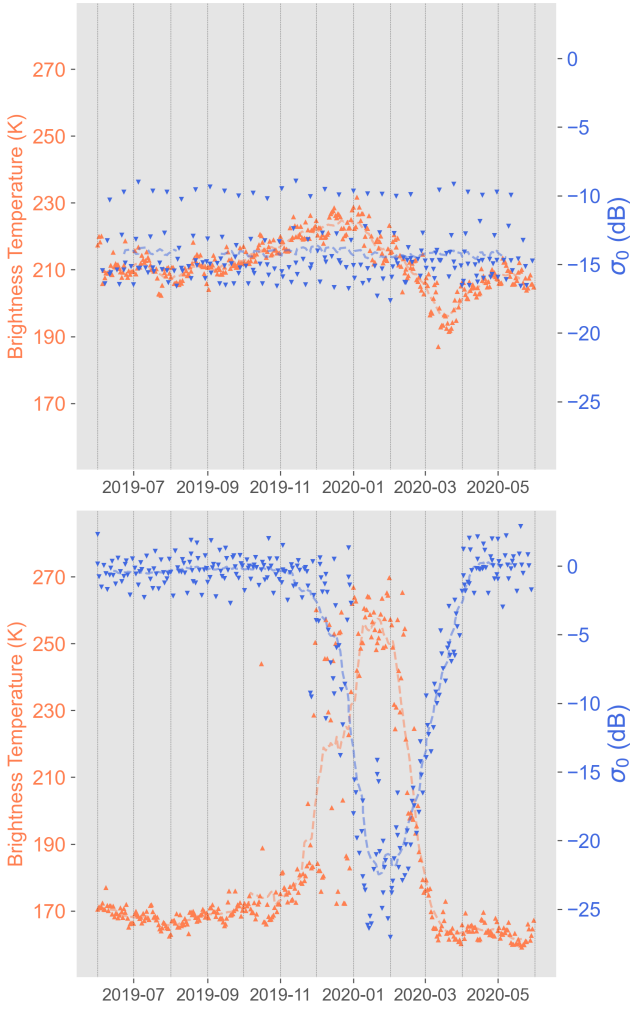

Figure 2. Evolution of backscattering coefficient σ_0 (in blue) and brightness temperature (orange) over the Larsen C ice shelf (top, 67.54°S 63.90°W) and the Wilkin coast (bottom, 68.08°S 65.86°W) over the 2019-2020 melt season. In a place where not melting is observed (top), σ_0 and the brightness temperature shows almost no changes. On the contrary, in areas subject to melt (bottom), we can observe a decrease of σ_0 and an increase in the observed brightness temperature.

a reduction of the discontinuities between the sub-swath, a radiometric calibration, and a terrain correction from the ASTER digital elevation model. The choice has been made to resample S1 images to a 1 km resolution using mean values before detecting melt. The data will ultimately be interpolated on the 7.5 km MAR grid. Before resampling, a 3x3 refined lee speckle filter developed by Mullissa et al. (2021) was applied to the images in addition to a radiometric terrain flattening using the 1 arc-minute global ETOP1 DEM (Amante and Eakins, 2009).

https://doi.org/10.5194/egusphere-2022-1371
Preprint. Discussion started: 15 December 2022

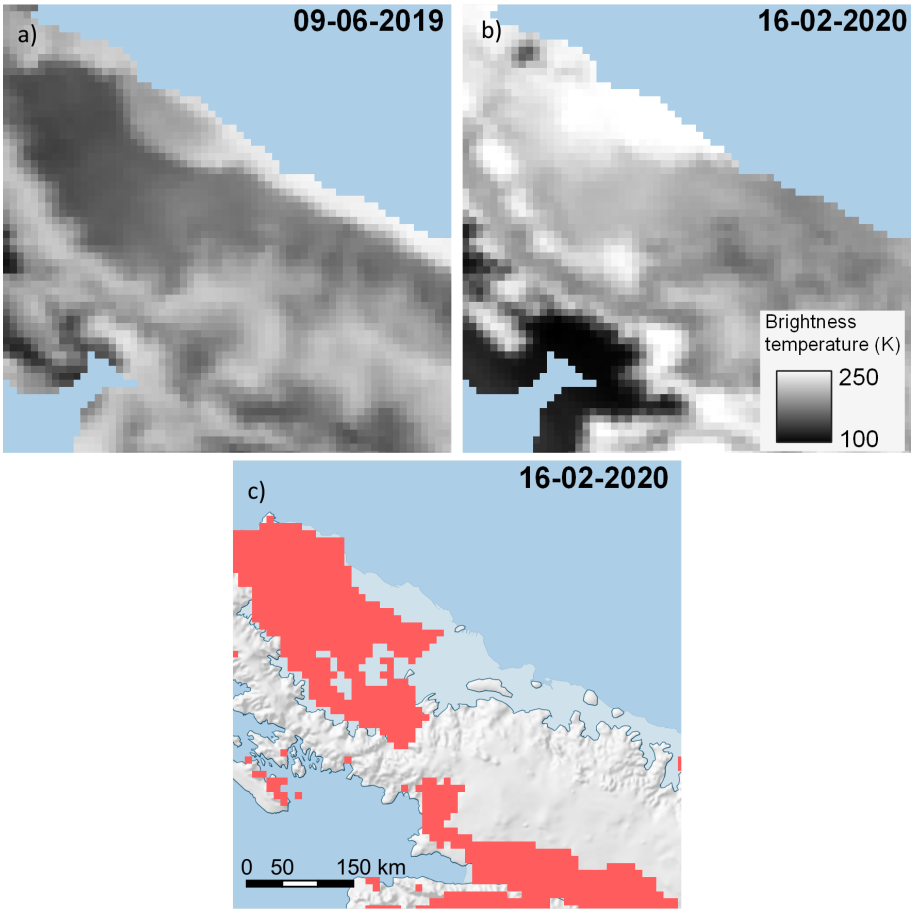

Figure 3. Detection of melt in an AMSR2 image over the Antarctic Peninsula. The increase in TB between a) and b) is interpreted as the presence of liquid water in the snowpack. After thresholding, the light red areas are pixels considered as melt.

After resampling, the images are normalized to their winter mean, using a technique called "co-orbit normalization" (Liang et al., 2021) or "winter-normalization". The winter mean is calculated with observations from June to October. Pixels with values lower than -28 dB were removed from the dataset. To deal with the changes in acquisition geometry, even if the images are supposed to be topography-free (terrain-corrected and terrain flattened), only the acquisitions from the same orbit and scene are taken into account to calculate the winter mean. Consequently, differences between the acquisitions are independent of the topography and the local context. The melt is then detected in the image by applying the -2.66 dB threshold (Figure 4), following Liang et al. (2021).

To create daily images of melt, images of the same day were combined. In case of overlapping images, the pixel-wise melt state is selected by a temporal majority filter. The acquisition time is defined as the mean time between the selected acquisitions. Else, if there are only two images that contradict each other, the non-melting status is assumed.

https://doi.org/10.5194/egusphere-2022-1371
Preprint. Discussion started: 15 December 2022

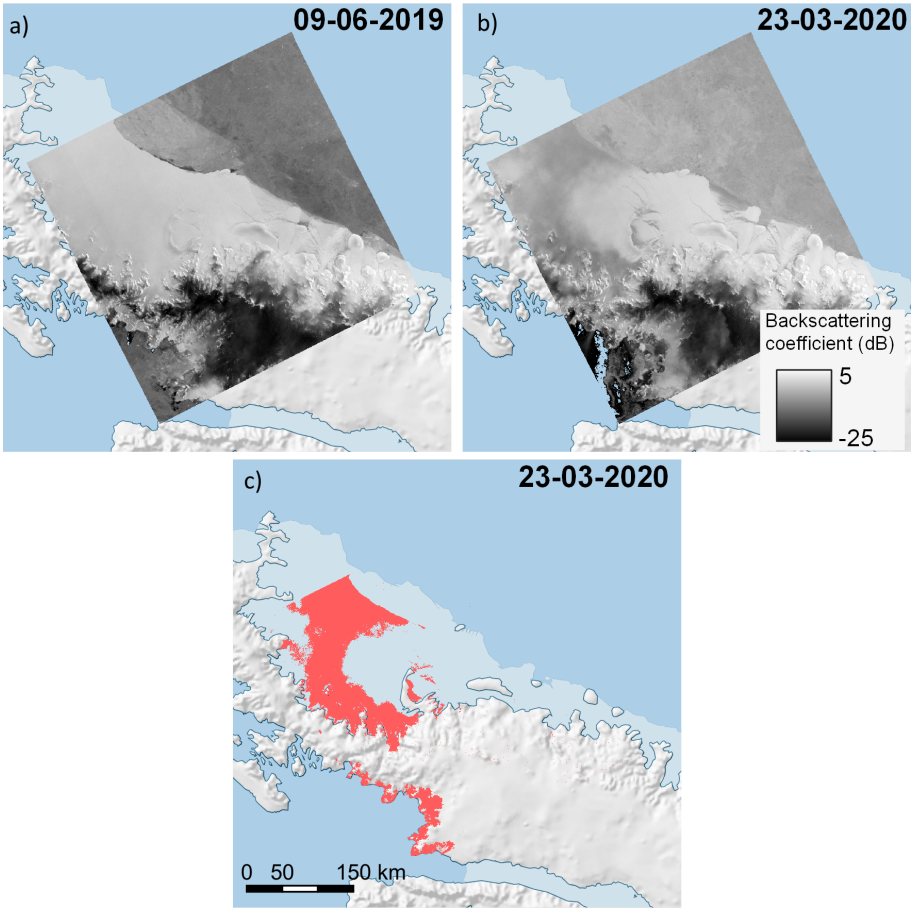

Figure 4. Detection of melt in a Sentinel-1 image over the Antarctic Peninsula. The decrease in backscatter between a) and b) is interpreted as the presence of liquid water in the snowpack. After thresholding, the light red areas are pixels considered as melt.

The third sensor we are using for this study is the C-band "Advanced Scatterometer" (ASCAT). After resolution enhancement (Lindsley and Long, 2016), it provides a backscattering coefficient at 4.45-km resolution by accumulating images over about 2 days. In Antarctica, only morning passes are selected for this process. The detection of the melt uses a simple threshold technique (Ashcraft and Long, 2006). The June-August mean backscattering coefficient is first calculated for each pixel and each year, and then every measurement lower than this mean -3 dB is considered as melting. Similar to AMSR2 daily products, the Sentinel-1 and ASCAT daily melt images are interpolated on the MAR grid.

2.2 The regional climate model

We employed the Regional Climate Model MAR. MAR is a polar-oriented regional climate model mostly used to study both the Greenland (Delhasse et al., 2020; Fettweis et al., 2021) and Antarctic ice sheet (Glaude et al., 2020; Amory et al., 2021; Kittel et al., 2021). Its atmospheric dynamics are based on hydrostatic approximation of primitive equations originally described

https://doi.org/10.5194/egusphere-2022-1371
Preprint. Discussion started: 15 December 2022

in Gallée and Schayes (1994) and the radiative transfer scheme is adapted from Morcrette (2002). The transfer of mass and energy between the atmospheric part of the model and the atmosphere is handled by the Soil Ice Snow Vegetation Atmospheric Transfer module (SISVAT, Ridder and Gallée, 1998), from which snow and ice albedo sub-modules are based on CROCUS (Brun et al., 1992). The model has been parameterized to resolve the topmost 20 meters of the snowpack, divided into 30 layers of time varying thickness. Each layer has a maximum water content holding capacity of 5 $\%$ beyond which the water freely percolates through the snowpack or runoffs above impermeable layers (bare ice or ice lenses).

For this work, MARv3.12 was used, including recent improvements in the snowpack temperature and the mass water conservation in soil as described in Lambin et al. (2022). MAR was run at a 7.5 km resolution over the Antarctic Peninsula, with a 40-second time step. It was forced at its lateral boundaries and over ocean by the 6-hourly ERA5 reanalysis (Hersbach et al., 2020) between March 2017 and May 2021. Snowpack was initialized in 2017 with a previous MAR simulation (Kittel et al., 2021). Finally, the simulations with assimilation were started in January 2019, restarting from the simulation without assimilation.

2.3 Data assimilation

The satellites sensors are sensitive to the presence of liquid water in the snowpack rather than the physical process of melt production. The aim of the data assimilation is then to guide or constrain the surface melt production of the model by nudging it to match the observed surface state. Correcting the melt occurrence influences the melt production at the same time. For computational reasons, the assimilation routine is called at each MAR time step only during the melting season, between October and April. Outside of this period, no assimilation is performed. The routine consists in comparing, pixel by pixel, the model and the satellites melt masks, and warms or cools the snowpack to fit the observations. The satellite acquisition time is used for the assimilation if the indicated acquisition time is separated by less than 1.5 hour from the MAR time. As three satellite products are assimilated at the same time, three separate cases have been developed. Each case is called according to the number of acquisitions that is taken into account in the routine (Figure 5).

The first case represents the situation where a single acquisition is available for the timestep. It is also the most frequent (between 90 and 95 $\%$ of the time depending on the year) and the basis for the others. This case is inspired by the assimilation performed in Kittel et al. (2022). For 3 hours around the observation (1.5 h before the observation and 1.5 after, so the model has time to adapt its behavior but the impact remains limited), at each MAR time step, the quantity of liquid water modeled within the pixel is compared to the RS-based mask. If the quantity of modeled liquid water is under a certain threshold (α) while the satellite mask indicates melt, first snow layers are heated by 0.15 $^{\circ}\mathrm{C}$ up to a certain depth (Δ_z) that depends on the sensor wavelength, until the melt threshold is reached. In contrast, if the water quantity is above the threshold α but no melt is observed by satellites, the snow is cooled down by the same rate of 0.15 $^{\circ}\mathrm{C}$ by MAR time step. However, in both cases, two conditions prevent the assimilation to change the MAR snowpack temperature. The first is that if the snow density is above 830 $\mathrm{km\,m^{-3}}$, the layer is considered as ice and the model does not permit liquid water to accumulate into ice. The temperature is then not changed as the threshold would never be reached. The second condition is the temperature of the snow layers above the Δ_z. If their mean temperature is under -7.5 $^{\circ}\mathrm{C}$, the MAR snowpack is too cold to have melt in the mode by warming its

https://doi.org/10.5194/egusphere-2022-1371
Preprint. Discussion started: 15 December 2022

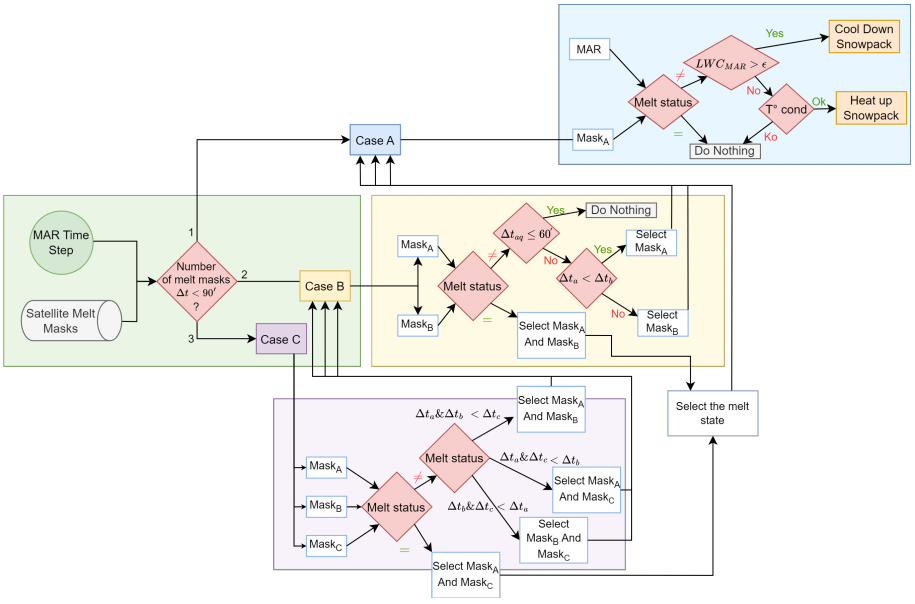

Figure 5. Flowchart of the assimilation algorithm. The number of satellite images available around the MAR time step determines the subprocess that is called in the routine. 3 subprocesses are defined: case A, case B, and case C. They respectively represent the availability of 1, 2, and 3 satellite images for the assimilation. The cases are funneling to case A so either the images do not give the same information and are discarded or multiple acquisition can be interpreted as one.

snowpack and the satellite observation is discarded. This operation is repeated until the observation is out of the time range. The choices for thresholds α and Δ_z are discussed in the two next sections, 2.3.1 and 2.3.2.

The second case is called when there are two satellite observations at less than 1.5 hours from MAR time. If the two masks have the same observation, *i.e.* no melt or melt, the two observations are associated with the first case but with a Δ_z equivalent to the mean values of the thresholds that would have been used for individual observations. If the two observations indicate different melt states, a different processing is applied if the acquisitions are close to each other in time (within an hour) or not. For two inconsistent observations distant by more than one hour, the assimilated melt state is the melt state from the closest image to the MAR time, following the first case. For two close contradictory observations, nothing is assimilated as they are considered both equally likely to be correct or wrong. The model is thus run as if there is no observation.

The third case is when all three observations are available at the same time. As for the second case, if the three masks agree with the same melt status, they are considered as one and as a longer first case. Again, Δ_z is equivalent to the mean values of the threshold that would have been used otherwise. If an observation is different from the other two, the two closest observations of the MAR time are analyzed using the second case described here above. For our configuration of sensors, this third case is only encountered a couple of times (less than 1 % of the time) while using AMSR2 (ascending orbit), ASCAT, and Sentinel-1, and so have virtually no implication on the melt estimation.

https://doi.org/10.5194/egusphere-2022-1371
Preprint. Discussion started: 15 December 2022

Before this case selection, if there are 3 satellite observations available for a pixel for a single day another criterion is applied. Following Picard and Fily (2006) demonstrating a daily cycle in brightness temperature, and thus surface melt, if melt is observed in the earliest and latest observation, an in-between observation with no melt is removed.

2.3.1 Choice of water content threshold α

Estimating the quantity of water in the snowpack with a single satellite acquisition is challenging. Despite the numerous research studies, the knowledge in the subject remains limited (Trusel et al., 2013; Fricker et al., 2021). However, as described in Picard et al. (2022), it is possible to find a typical water quantity for which the satellite signal significantly changes, and can be detected as melting. Picard et al. (2022) shows that a very small amount of water can be detected with the radio frequencies used in this study. Only 0.11 and 0.05 $\mathrm{km\,m^{-2}}$ are necessary at respectively 6 GHz and 19 GHz if the water is uniformly spread over the pixel. This quantity can be higher for heterogeneous pixels containing patches with and without melt. For this study, the choice has been made to use the same threshold no matter the sensor frequency. The passive microwave sensors acquired at higher frequencies are in principle more sensitive, but having a coarser resolution than that of the two active sensors, their pixels tend to be more heterogeneous, suggesting a compensation. Two thresholds have been proposed to significantly change the snowpack brightness temperature in the literature. Tedesco et al. (2007) proposed a threshold of 0.2 % when Picard et al. (2022) proposed 0.1 %. They both have been tested in Kittel et al. (2022) the choice was found to not significantly influence the melt quantity produced by the MAR model. The sensitivity of the microwave is high enough that the quantities of liquid water that can be detected is much smaller than that produced during a typical melting day (1.2 ± 0.6 % as modeled by MAR over the studied zone).

2.3.2 Choice of penetration depth threshold Δ_z

Microwaves have penetration capabilities directly related to their wavelength (Elachi and van Zyl, 2006). As a consequence, C-band SAR from Sentinel-1 has a different penetration depth than Ku-band from AMSR2. In addition, the water content strongly influences the penetration depth, as water at the top of the snowpack can prevent deeper penetration (Fig. 6). In this experiment, we set different limits of penetration for each remote sensing product to test its influence. Using AMSR2 (Ku-Band), we consider a depth Δ_z = 0.1, 0.2, and 0.4 m successively below the surface. Below this depth, the electromagnetic wave should not have a noticeable influence (Picard et al., 2022). For Sentinel-1 and ASCAT (C-band), the depth threshold Δ_z is set up to 0.5, 1, and 1.5 m.

3 Evaluation

Because the integrated physics within RCMs are either partially resolved or contain uncertainties, it is first required to evaluate models outputs to in situ measurements. The evaluation is there to quantify how close the model is to reality and if the model is inclined to reproduce this observed situation.

https://doi.org/10.5194/egusphere-2022-1371
Preprint. Discussion started: 15 December 2022

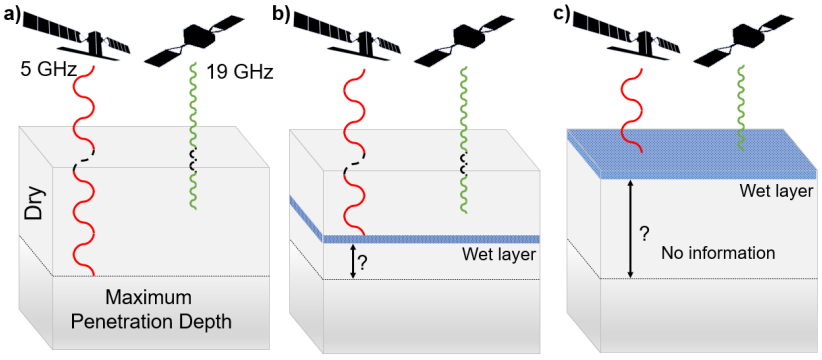

Figure 6. Illustration of the penetration depth of the microwave sensor according to their wavelength and the depth of the wet snow layer. (a) Penetration depth in a dry snowpack. The signal of the sensor with the lower frequency (5 GHz) penetrates deeper than the signal of the higher one (19 GHz). (b) Penetration depth with a layer of liquid water deep in the snowpack. The microwave sensor with deeper penetration is able to detect melt but the other cannot. (c) Penetration depth with liquid water at the top of the snowpack. Both satellites can observe the presence of liquid water.

The outputs of the model are evaluated by comparing some modeled variables with in situ observations. The daily observations are provided by Automatic Weather Stations (AWS) widespread across the AIS. Here, 9 weather-stations datasets available in the studied zone (blue crosses displayed in Fig. 1) have been gathered to calculate statistics between the model and the observations as done in Kittel (2021) and Mottram et al. (2021). The statistics employed for the evaluation are the Mean Bias (MB), Root Mean Square Error (RMSE), Centered Root Mean Square Error (CRMSE), and correlation (Table 1). The statistics are listed for the 2016-2021 period for the near surface pressure, temperature, wind speed, relative humidity, short-wavelength downward radiations (SWD), short-wavelength upward radiations (SWU), long-wavelength downward radiations (LWD), and long-wavelength upward radiations (LWU).

Small biases can exist between the observations and the model due to the elevation difference. The observations are punctual when the model provides zonal information over a 7.5 x 7.5 km^2 pixel. Thus the mean elevation of the MAR pixel in which the AWS falls is not the same as the AWS true elevation. This difference is particularly noticeable for the near-surface pressure, directly linked to the elevation. Nonetheless, a high correlation ($r > 0.98$) reflects the MAR ability to simulate its temporal variability.

In general, the winter season is slightly better represented with higher correlations and lower mean bias than the summer season. Larger differences are observed in summer for long-wavelength downward radiations LWD ($r = 0.65$). This difference is compensated by the excess of short-wavelength solar radiations over the year. As explained in Delhasse et al. (2020), MAR is outperformed by reanalysis when representing downward radiative fluxes. MAR does not assimilate temperature profile nor coastal temperature but is only forced at its boundaries every 6h for its specific humidity and temperature. Thus modeled clouds are the outcome of the model climate and microphysics (Delhasse et al., 2020). Moreover, the radiative scheme implemented

https://doi.org/10.5194/egusphere-2022-1371
Preprint. Discussion started: 15 December 2022

Table 1. Mean Bias (MB), Root Mean Square Error (RMSE), Centered Root Mean Square Error (CRMSE), and correlation between MAR and daily observation over the Antarctic Peninsula. A negative value implies a lower MAR estimate than the observation. Statistics are given for the for the near surface pressure, temperature, wind speed, relative humidity, shortwave downward (SWD), shortwave upward (SWU), longwave downward (LWD), and longwave upward (LWU) annually, for the summer (DJF), and for the winter (JJA) and are calculated for the 2016-2021 period. During winter, the absence of the Sun implies no short-wavelength solar radiation measurements (SWD and SWU). Locations of the weather station used for the daily observations are marked by blue crosses in Fig. 1.

	Annual				Summer				Winter			
	MB	RMSE	CRMSE	Correlation	MB	RMSE	CRMSE	Correlation	MB	RMSE	CRMSE	Correlation
Near Surface Pressure (hPa)	-5.44	14.57	1.25	0.99	-5.69	13.18	0.87	0.99	-6.13	16.09	1.42	0.99
Temperature (°C)	-0.32	3.32	2.81	0.93	-1.13	2.36	1.68	0.76	0.3	3.63	3.11	0.92
Wind speed ($\mathrm{m\,s_{-1}}$)	-0.39	2.58	2.28	0.79	-0.43	2.22	1.85	0.7	-0.35	2.92	2.57	0.78
Relative humidity (%)	3.2	8.73	8.13	0.72	6.88	9.32	6.29	0.75	2.87	9.1	8.64	0.79
SWD ($\mathrm{W\,s_{-2}}$)	13.87	36.23	33.46	0.97	41.58	59.21	42.15	0.79	/	/	/	/
SWU ($\mathrm{W\,s_{-2}}$)	-0.2	24.04	24.04	0.97	14.38	35.81	32.8	0.78	/	/	/	/
LWD ($\mathrm{W\,s_{-2}}$)	-14.75	26.15	21.59	0.76	-26.56	32.51	18.75	0.65	-7.12	21.08	19.85	0.81
LWU ($\mathrm{W\,s_{-2}}$)	3.4	14.2	13.79	0.93	-0.52	9.2	9.19	0.76	2.83	17.12	16.88	0.9

in MAR is the one from the ERA-40 reanalysis. This scheme has been updated in the ERA-interim and ERA-5 reanalysis (Hersbach et al., 2018, 2020) but not in the model. Combined with cloud physics, bias in downward radiative fluxes can appear in MAR.

4 Results

The results of an ensemble of twenty MAR simulations is presented here. The reference MAR simulation, MAR_{ref}, is performed without assimilation. The 19 others are referred to as "assimilations" hereafter. For each one, the satellite melt masks are assimilated into the model, with different parameters (Table 2). The reference assimilation ($Assim_{ref}$) is using Sentinel-1 and AMSR2, both their ascending and descending orbits, and with thresholds Δ_z = 1 m and 0.2 m respectively. Also, α is set at 0.1 %. The thresholds of $Assim_{ref}$ correspond to values given in the literature (Elachi and van Zyl, 2006; Picard et al., 2022). The sensitivity tests have been performed from June 2019 to May 2020, and from June 2020 to May 2021. The 2020-2021 season graphs are available in Supplementary materials.

The evolution of several variables (Table 3) including surface Melt (ME), Runoff (RU), Surface Mass Balance (SMB), Snowpack Density (ρ), and Liquid Water Content (LWC), is analyzed to study the changes to the model caused by the data assimilation. The first 3 variables (ME, RU, and SMB) are given for the entire snowpack profile while the other two ρ and LWC) are taken at 0.2- and 1-meter depth. The average value of the variables of all the assimilations, $Assim_{mean}$, is compared to the model with no assimilation. Although $Assim_{mean}$ gives different results from the reference assimilation, $Assim_{ref}$ is the closest simulation to $Assim_{mean}$.

https://doi.org/10.5194/egusphere-2022-1371
Preprint. Discussion started: 15 December 2022

Table 2. Name of the different simulation and parameterization of the simulation with data assimilation. Simulations marked with an asterisk have been removed from the calculation of the ensemble average.

	α (%)	Ku band Δ_z (m)	C-band Δ_z (m)	Sensors
$Assim_{ref}$	0.1	0.2	1	AMSR2 + S1
$MAR_{a01-ku02-c05}$	0.1	0.2	0.5	AMSR2 + S1
$MAR_{a01-ku02-c15}$	0.1	0.2	1.5	AMSR2 + S1
$MAR_{a02-ku02-c10}$	0.2	0.2	1	AMSR2 + S1
$MAR_{a02-ku02-c05}$	0.2	0.2	0.5	AMSR2 + S1
$MAR_{a02-ku02-c15}$	0.2	0.2	1.5	AMSR2 + S1
$MAR_{a01-ku01-c10}$	0.1	0.1	1	AMSR2 + S1
$MAR_{a01-ku01-c05}$	0.1	0.1	0.5	AMSR2 + S1
$MAR_{a01-ku01-c15}$	0.1	0.1	1.5	AMSR2 + S1
$MAR_{a02-ku01-c10*}$	0.2	0.1	1	AMSR2 + S1
$MAR_{a02-ku01-c05*}$	0.2	0.1	0.5	AMSR2 + S1
$MAR_{a02-ku01-c15*}$	0.2	0.1	1.5	AMSR2 + S1
$MAR_{a01-ku04-c10}$	0.1	0.4	1	AMSR2 + S1
$MAR_{a01-ku04-c05}$	0.1	0.4	0.5	AMSR2 + S1
$MAR_{a01-ku04-c15}$	0.1	0.4	1.5	AMSR2 + S1
$MAR_{a02-ku04-c10}$	0.2	0.4	1	AMSR2 + S1
$MAR_{a02-ku04-c05}$	0.2	0.4	0.5	AMSR2 + S1
$MAR_{a02-ku04-c15}$	0.2	0.4	1.5	AMSR2 + S1
$MAR_{a01-ku02-c10}$	0.1	0.2	1	AMSR2 (asc.) + S1 + ASCAT
MAR_{ref}	/	/	/	None

Table 3. Surface mass balance (SMB), and average snowpack density (ρ) and snowpack liquid water content (LWC) for MAR_{ref}, the reference assimilation ($Assim_{ref}$) and the mean value of the assimilations ($Assim_{mean}$) over the Antarctic Peninsula for the 2019-2020 melt season. The range comprises all 19 assimilations. LWC and ρ are taken at a depth of 0.2 m and 1 m while the other variable are given as a snowpack cumulated value.

	ME (Gt yr^{-1})	RU (Gt yr^{-1})	SMB (Gt yr^{-1})	$\rho_{0.2\mathrm{m}}$ (kgm^{-3})	$\rho_{1\mathrm{m}}$ (kgm^{-3})	$LWC_{0.2\mathrm{m}}$ (kgkg^{-1})	$LWC_{1\mathrm{m}}$ (kgkg^{-1})
MAR_{ref}	142	32	451	447	434	0.004	0.005
$Assim_{ref}$	214	56	427	480	456	0.003	0.005
$Assim_{mean}$	237	53	431	481	457	0.003	0.005
Range	183 - 299	45 - 60	424 - 439	472 - 490	451 - 463	0.003 - 0.004	0.004 - 0.007
Evolution (%)	66.7	63.8	-4.5	7.4	5.2	-8.1	-2.2

Although there are divergences while using different parameters in the assimilation, the surface melt production is larger compared to MAR_{ref} for all assimilations. On average, the melt extent provided by the melt masks are larger than the melt

https://doi.org/10.5194/egusphere-2022-1371
Preprint. Discussion started: 15 December 2022

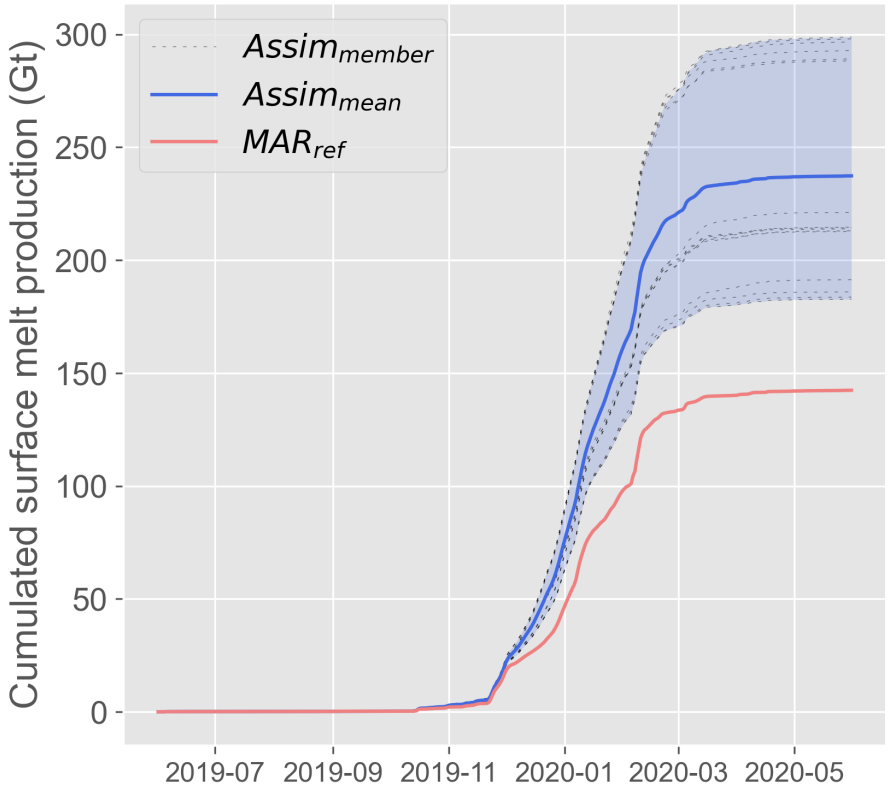

Figure 7. Cumulated surface melt production (Gt) for the 2019-2020 melt season as modeled by MAR without assimilation (MAR_{ref} in light red), with data assimilation ($Assim_{member}$ in dashed lines), and their averaged value ($Assim_{mean}$ in blue). Shaded areas represent the range of the assimilations.

extent modeled by MAR_{ref} on the Antarctic Peninsula. This difference impacts the melt production in the model (Fig. 7). No matter the parametrization of the assimilation, the surface melt production is increased compared to MAR_{ref}, leading to an cumulated melt production increase of 63.8 % for the $Assim_{mean}$.

The snowpack can saturate, either from meltwater production or from densification. If snowpack liquid water content exceeds 5 %, the excess water starts to trickle and run off. In Antarctica, runoff is driven by the surface melt production and rainfall (Gilbert and Kittel, 2021). The evolution of runoff is thus directly related to the evolution of melt and the snowpack saturation level. Nonetheless, if the relative evolution between $Assim_{mean}$ and MAR_{ref} is the same for surface melt and runoff (+66.7 % and +63.8 % respectively), it is not the case in absolute (+95 $\mathrm{Gt\,y^{-1}}$ and +21 $\mathrm{Gt\,y^{-1}}$). In other words, the snowpack is still able to absorb liquid water as long as it is not fully saturated. The strongest increase in runoff occurs together with firn air content depletion over the ice shelves. Liquid can stay in the porous layers of the surface snowpack. Then, depending on the temperature and the melt production, the water either refreezes during the night or percolates deeper in the snowpack.

https://doi.org/10.5194/egusphere-2022-1371
Preprint. Discussion started: 15 December 2022

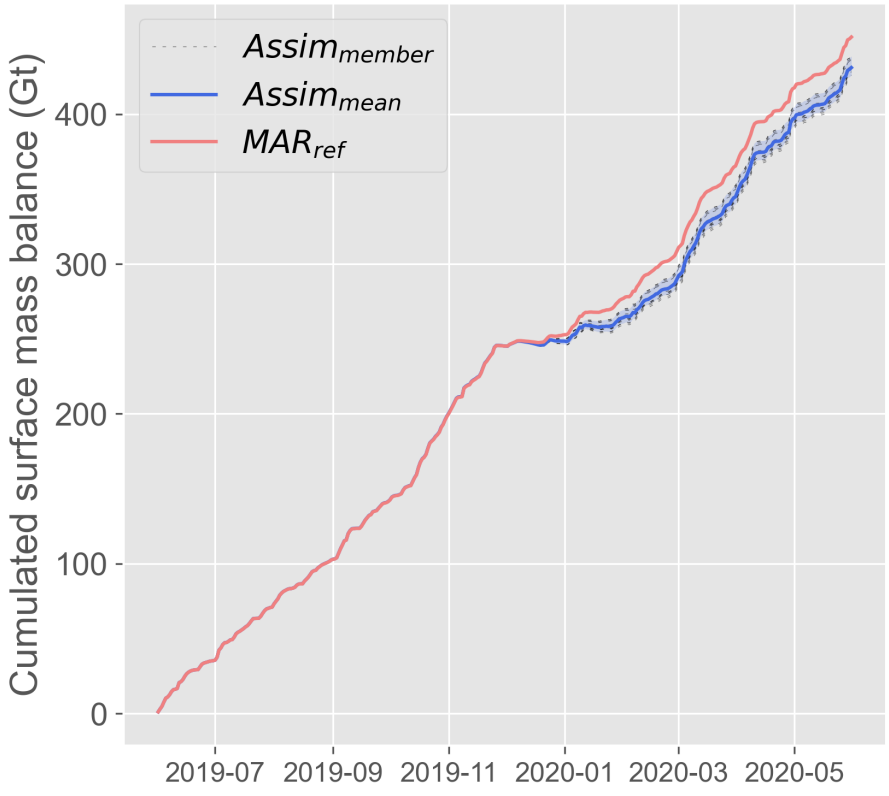

Figure 8. Cumulated surface mass balance (Gt) for 2019-2020 melt season as modeled by MAR without assimilation (MAR_{ref} in red), with data assimilation ($Assim_{member}$ in dashed lines), and their averaged value ($Assim_{mean}$ in blue). Shaded areas represent the range of the assimilations.

By refreezing, the water densify the firn, causing firn air content depletion, leaving less storage space for liquid water in the perennial snowpack (Banwell et al., 2021).

As it can be seen in Fig. 8, the data assimilation only has a slight effect on the SMB. The surface mass balance is defined as the sum of the ablation terms (runoff, melt, and sublimation) and accumulation terms (*e.g.* precipitation and snow transported by the wind). The cumulated SMB for the 2019-2020 melt season is only decreased by 4.5 % compared to the model without assimilation. The general trend of SMB remains positive in the studied zone. Only the ice shelves show negative SMB during periods of intense melting (Fig. 9).

The density and liquid water content of the snowpack are also impacted by the assimilation. As presented in Table 4, on the ice shelves, where most of the surface melt and refreezing occurs, densification has an effect on the deeper liquid water content. Because the snowpack is denser, there is less space for liquid water and thus the liquid water quantity in the snowpack is lower after assimilation.

https://doi.org/10.5194/egusphere-2022-1371
Preprint. Discussion started: 15 December 2022

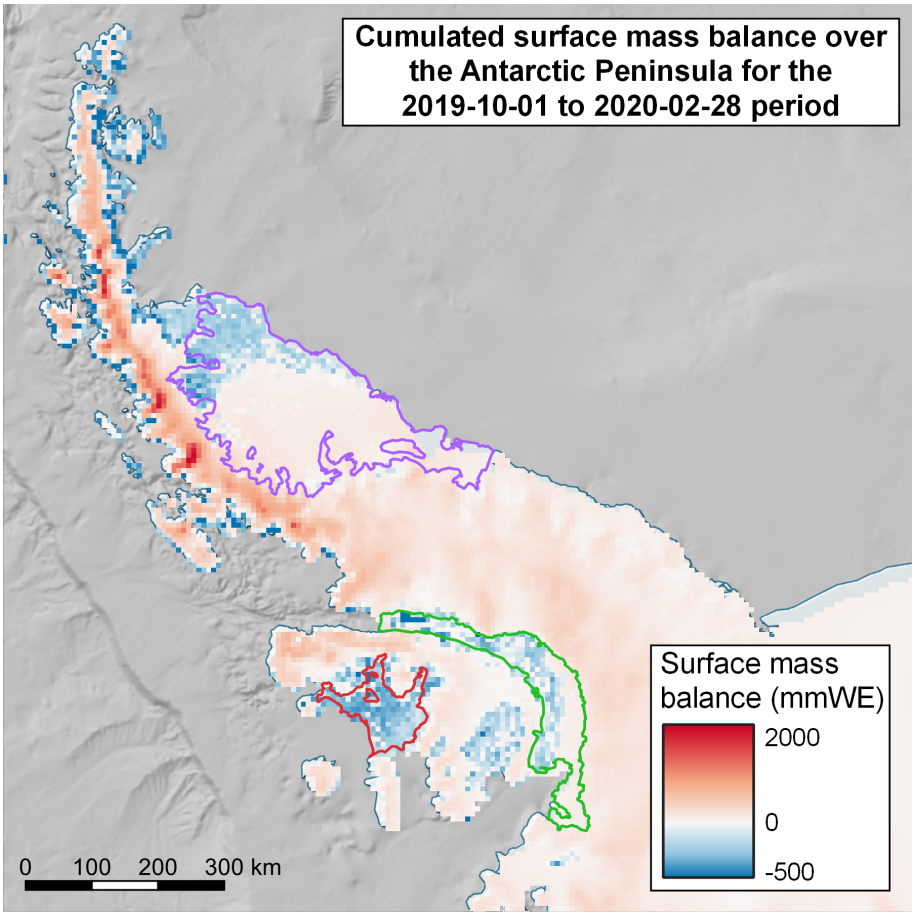

Figure 9. Cumulated SMB (mmWE) from 2019-10-01 to 2020-02-28 over the AP as modeled by $Assim_{ref}$. Larsen C is outlined in purple, Georges VI in green, and Wilkins in red. The ice shelves and the northernmost coastlines are experiencing a decrease in SMB in opposition to the rest of the AP.

For the three highlighted ice shelves (Larsen C, Wilkins, and Georges VI), the evolution follows the same general trend as for the global zone but at different speeds (Table 4). The only exception is that even if Larsen C is the ice shelf experiencing the higher increase of melt (+20 $\mathrm{Gt\,y^{-1}}$), and consequently runoff (+5.7 $\mathrm{Gt\,y^{-1}}$), both its liquid water content at 0.2 m depth and 1m depth is increasing instead of decreasing (respectively +4 $\%$, and +12 $\%$).

With the exception of the liquid water content, the changes in the snow related variables of the model are so strong that MAR_{ref} is out of the range of the different assimilations. The increase in surface melt production leads to an increase in the runoff and consequently a decrease in surface mass balance. The increase in runoff is explained by the densification of the first layers of the snowpack and thus the decrease of its ability to buffer for the meltwater.

In the end, the results illustrate that $Assim_{ref}$ is the closest simulation to $Assim_{mean}$, and makes it an appropriate candidate when computational resources are limited.

https://doi.org/10.5194/egusphere-2022-1371
Preprint. Discussion started: 15 December 2022

Table 4. Evolution of surface melt production (ME), runoff (Ru), surface mass balance (SMB), snowpack density (ρ), and snowpack liquid water content (LWC) for MAR_{ref}, the reference assimilation ($Assim_{ref}$) and the mean value of the assimilations ($Assim_{mean}$) over the 3 studied ice shelves for the 2019-2020 melt season. LWC and ρ are given at a depth of 0.2 m and 1 m while the other variable are given as a snowpack average value.

Larsen C	ME ($\mathrm{Gt\,yr^{-1}}$)	RU ($\mathrm{Gt\,yr^{-1}}$)	SMB ($\mathrm{Gt\,yr^{-1}}$)	$\rho_{0.2\mathrm{m}}$ ($\mathrm{kg\,m^{-3}}$)	$\rho_{1\mathrm{m}}$ ($\mathrm{kg\,m^{-3}}$)	$LWC_{0.2\mathrm{m}}$ ($\mathrm{kg\,kg^{-1}}$)	$LWC_{1\mathrm{m}}$ ($\mathrm{kg\,kg^{-1}}$)
MAR	23	1.8	24	519	554	0.00097	0.00060
$Assim_{ref}$	38	6.6	19	570	612	0.00099	0.00066
$Assim_{mean}$	44	7.5	19	575	614	0.00101	0.00067
σ	11	2.1	2.2	55	47	0.00091	0.00063
Wilkins	ME ($\mathrm{Gt\,yr^{-1}}$)	RU ($\mathrm{Gt\,yr^{-1}}$)	SMB ($\mathrm{Gt\,yr^{-1}}$)	$\rho_{0.2\mathrm{m}}$ ($\mathrm{kg\,m^{-3}}$)	$\rho_{1\mathrm{m}}$ ($\mathrm{kg\,m^{-3}}$)	$LWC_{0.2\mathrm{m}}$ ($\mathrm{kg\,kg^{-1}}$)	$LWC_{1\mathrm{m}}$ ($\mathrm{kg\,kg^{-1}}$)
MAR	9.5	1.5	5.5	630	628	0.00035	0.00027
$Assim_{ref}$	13	5.4	1.6	697	689	0.00026	0.00022
$Assim_{mean}$	14	4.4	2.7	683	685	0.00027	0.00022
σ	3	1.4	1.4	69	101	0.00017	0.00011
Georges VI	ME ($\mathrm{Gt\,yr^{-1}}$)	RU ($\mathrm{Gt\,yr^{-1}}$)	SMB ($\mathrm{Gt\,yr^{-1}}$)	$\rho_{0.2\mathrm{m}}$ ($\mathrm{kg\,m^{-3}}$)	$\rho_{1\mathrm{m}}$ ($\mathrm{kg\,m^{-3}}$)	$LWC_{0.2\mathrm{m}}$ ($\mathrm{kg\,kg^{-1}}$)	$LWC_{1\mathrm{m}}$ ($\mathrm{kg\,kg^{-1}}$)
MAR	15	2	11	567	607	0.00058	0.00040
$Assim_{ref}$	20	3.4	9.6	618	641	0.00052	0.00040
$Assim_{mean}$	22	3.1	10	607	638	0.00056	0.00042
σ	5.1	0.4	0.4	59	58	0.00029	0.00029

4.1 Penetration Depth Sensitivity

The penetration depth influences melt production. For the assimilation, we are using a relative liquid water mass in relation to the snowpack weight. Because of the refreezing, the first 10 centimeters of the snowpack are denser than the first meter. Consequently, when using a shallow threshold, the quantity of water required to reach the threshold will be greater as the densification will eventually cause a heavier snowpack. Also, with firn air depletion, two other phenomena enhance the melt production. First, the available energy is consumed by refreezing/melting processes, prevailing the snowpack to heat up. A colder snowpack produces less melt and constantly needs larger forcing to reach the melt threshold. Second, because the upper layers are saturated with less water in the bottom layers, the runoff increases during melt events, and the remaining water percolates faster in the deeper layers. If the model would keep liquid water for a longer time in its top snow layers, less melt production would be necessary to match the observations.

This phenomenon is illustrated in Fig. 10, where using a 10 cm threshold for AMSR2 gives double the melt of the 20 cm threshold, either the water content threshold is 0.1 % or 0.2 %. The effect ends up so important that using a 10 cm threshold for ASMR can result in improbable results. Consequently, the three simulations with Δ_z = 10 cm for the Ku-band sensors have been discarded to calculate the average melt for the assimilations. The intense refreezing and firn air content depletion lead to a strong increase in runoff that causes a decrease in SMB for the Antarctic Peninsula. This evolution is in contradiction with

https://doi.org/10.5194/egusphere-2022-1371
Preprint. Discussion started: 15 December 2022

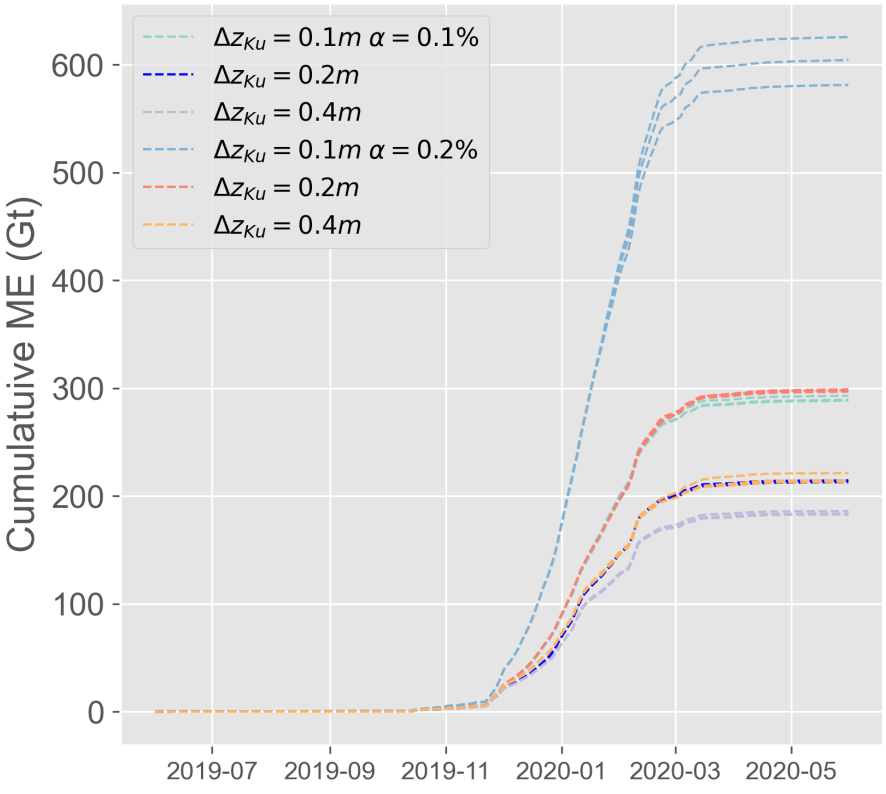

Figure 10. Cumulated surface melt production (Gt) for 2019-2020 melt season as modeled by the different assimilation. Curves of the same color have different Δ_z for the C-band sensors.

the observed trend that is generally accepted (Rignot et al., 2019; Kittel et al., 2021; Chuter et al., 2022). They were considered outliers and removed from the analysis of the results.

In contrast, with Sentinel-1, the effect of choosing a different threshold is less pronounced. As illustrated in Fig. 10, lines with the same color represent assimilations that have all parameters in common except the S1 penetration threshold. Almost no variation can be observed between the group of assimilation.

Multiple reasons can explain the lighter effect. S1 has a much larger revisit time compared to AMSR2 (6 days revisit time vs daily images). With fewer images, the choice of penetration depth is less often considered in the melt assimilation process in MAR. In addition, as explained previously, the liquid water is kept longer in these slightly deeper layers and thus no melt is required to reach the water quantity threshold. The model is thus more sensitive to a shallower penetration depth threshold. The sensitivity is linked to near-surface events, more likely to occur in the first centimeter of the snowpack. The penetration depth for the C-band sensors is larger than for Ku-band sensors, using sensors with higher frequencies makes the threshold choice more sensitive.

https://doi.org/10.5194/egusphere-2022-1371
Preprint. Discussion started: 15 December 2022

Table 5. Comparison between the melt season length and number of melt days modeled for the three studied ice shelves for MAR_{ref} and the assimilations for the 2019-2020 melt season.

Larsen C	Melt season length (days)	Number of melt days modeled
MAR_{ref}	143	90
α = 0.1 %	147	110
α = 0.2 %	152	119
Wilkins	**Melt season length (days)**	**Number of melt days modeled**
MAR_{ref}	292	127
α = 0.1 %	294	125
α = 0.2 %	298	129
GeorgesVI	**Melt season length (days)**	**Number of melt days modeled**
MAR_{ref}	120	120
α = 0.1 %	123	122
α = 0.2 %	157	134

4.2 Water content sensitivity

The water content sensitivity has a lesser impact compared to the penetration depth. In fact the required amount of liquid water to reach the thresholds is small compared to a typical melt day. For the 2019-2020 melt season, the value reaches 1.2 % for a melt day on average, far above the 0.2 % threshold. Choosing a threshold over the other mostly influences the number of melt days modeled, thus expanding the melt season duration (Table 5) rather than the mass of liquid water produced by melting. For this study, the melt season length is defined as the number of days between the first day of the year where more than 10 % of the ice shelf is experiencing melt. The melt season is different from the number of melt days of the ice shelf that is defined as the number of days of the melt season where 10 % of the ice shelf is experiencing melt, with possible colder periods where no melting event occurs.

Using a higher threshold results in an increase in the average number of melt days on the studied ice shelves (Fig. 11). The increase in melt days between the 0.1 and 0.2 % threshold is caused by the definition of a melt day we used. A pixel is considered as melting for the day if the average mass of liquid water is superior to 0.1 % of the snowpack mass. The definition is close to the one used for the assimilation except that the water mass is averaged for the days rather than taking an instantiate value. Using a higher threshold in the assimilation eventually leads to more melt production and thus a higher averaged value for the day.

The biggest difference occurs on Larsen C with an augmentation of the mean number of melt days on the ice shelf by 15 days. For the other two ice shelves, the differences are smaller with 8 and 9 days for Wilkins and Georges VI, respectively. Similar conclusions can be drawn when using 0.2 % for the definition of melt days.

Taking the assimilation individually leads to a similar conclusion. The water content threshold choice only emphasizes the differences that are caused by the penetration depth threshold. It is important to note that the simulations that were discarded

https://doi.org/10.5194/egusphere-2022-1371
Preprint. Discussion started: 15 December 2022

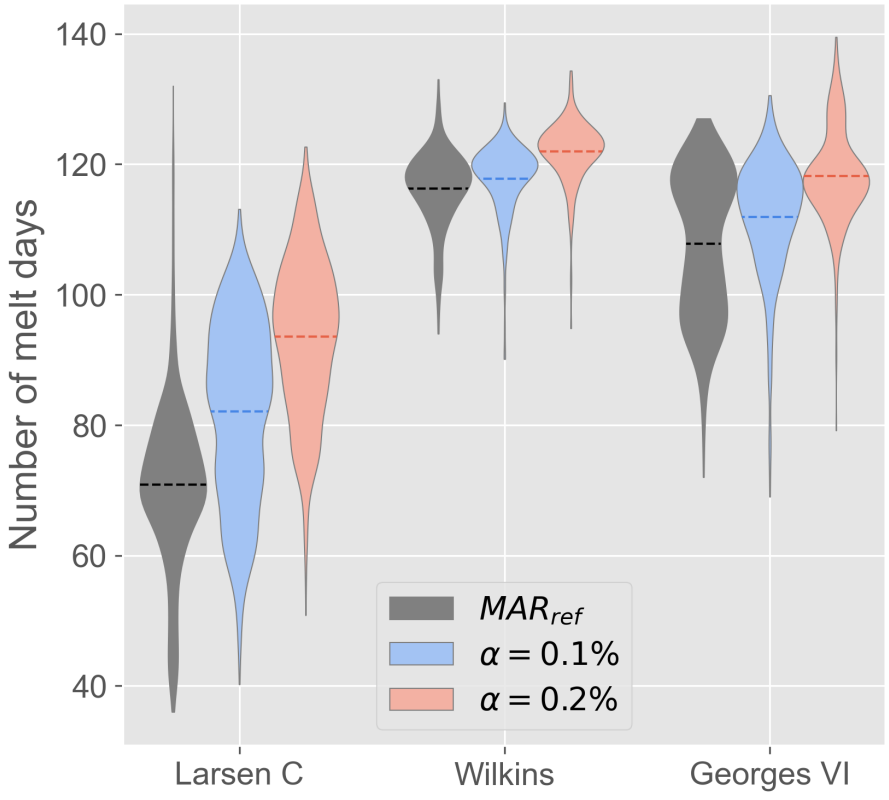

Figure 11. Distribution of the number of melt days fot the 2019-2020 melt season as modeled by MAR_{ref} and the assimilations for the two values of α for the three studied ice shelves. Dashed lines represent the mean value of the distribution.

from the computation of $Assim_{mean}$ are assimilation that had 0.2 % as the value for the threshold. With a densified snowpack, reaching α = 0.2 % required more intense melting.

4.3 Dataset sensitivity

The melt datasets used can be highly influential on the results. For a given period, MAR snowpack temperature is forced until a certain level of liquid water in the snowpack is reached in case of a mismatch between the model and the dataset.

Each of the four melt masks has been assimilated individually into MAR to test its influence. Assimilating multiple datasets tend to smooth the sensor characteristics as they are processed to be used where they provide consistent information.

In this study, several characteristics of the remote sensing data have been pinpointed as they influence the results of the assimilation. The acquisition time, the resolution, and the revisit time are discussed hereafter.

First, the acquisition time can artificially lower the number of melt days. Because of the daily cycle of the water quantity in the snowpack, images taken earlier in the morning are less likely to observe melt (Picard and Fily, 2006). In this manner, over

https://doi.org/10.5194/egusphere-2022-1371
Preprint. Discussion started: 15 December 2022

the Antarctic Peninsula, the descending orbit of AMSR2 observes less melt than the ascending one. Using satellites whose passage times are well distributed during the day allows them to observe this cycle and not miss melt days.

Second, the way spatial resolution influences the results of the assimilation is trivial. Sensors that have coarser resolution have more heterogeneous pixels and consequently detect melt in places that they should not (and inversely). In this study, AMSR2 is the only sensor to have a coarser resolution than the model and whose spatial resolution can be seen in the assimilation results.

To study its influence, ASCAT has been assimilated ($MAR_{a01-ku02-c10}$ in Table 2) instead of AMSR2 in descending orbit. The two assimilations gave similar numbers of melt days and close surface melt production on the Peninsula ice shelves (191 $\mathrm{Gt\,y^{-1}}$ for $MAR_{a01-ku02-c10}$ and 214 $\mathrm{Gt\,y^{-1}}$ for $Assim_{ref}$). The major influence for this case comes from the spatial resolution of the sensor. AMSR2 detects melt on Alexander island, between Georges VI and Wilkins ice shelves, when ASCAT with a finer resolution and other frequency does not (Fig. 12). With assimilation that uses AMSR2 in ascending and descending orbit, the model ends up melting there. On the contrary, the assimilation taking ASCAT data into account does not force MAR for a long enough time to produce the water quantities necessary to be detected as a melt day at these places.

Finally, the requirement of the low revisit time is highlighted with the assimilation of Sentinel-1 only. The results of the assimilation are close to the MAR_{ref} results (Fig. 13). The resilience of the model is too strong to only use a non-daily dataset. The nudging applied cannot induce significant changes by being applied every couple of days. Thus, the high spatial resolution of Sentinel-1 is not sufficient enough for it to be used as the only dataset assimilated. However, Sentinel-1 data can be used in complementarity to other datasets to solve the ambiguity problems induced by their spatial resolution.

For now, the restrained period during which the snowpack temperature is modified as well as the possibility not to assimilate data in case of discrepancy between the sensors reduce the sensibility to the data set used. Future developments of the technique should allow the inclusion of more datasets during the run.

5 Discussion and conclusion

In this paper, we presented the assimilation of surface melt occurrence estimated by microwave sensors into the regional climate model MAR. Sensitivity tests have been performed to evaluate the effect of the data assimilation parameters on the model results.

We identified the depth to which the snowpack temperature (Δ_z) as the most influential parameter when applied for low penetration sensors. The influence on the quantity of water produced in the snowpack partially comes from the water content threshold (α) calculation. The very first centimeters of the snowpack are very dense compared to slightly deeper layers because of refreezing induced by the liquid meltwater caused by the assimilation and the low temperature at night. Heavier and denser layers require more liquid water to reach the required threshold α. Also, the densification causes firn air content depletion, leaving less space for liquid water. Densified, the layer saturates faster and more runoff occurs.

However, the assimilation of surface melt occurrence has a small impact on the atmosphere. With constant snowfall and an increase in the surface melt (+95 $\mathrm{Gt\,y^{-1}}$ or +66.7 %), the increase in runoff (+21 $\mathrm{Gt\,y^{-1}}$ or +63.8 %) translates into a decrease

https://doi.org/10.5194/egusphere-2022-1371
Preprint. Discussion started: 15 December 2022

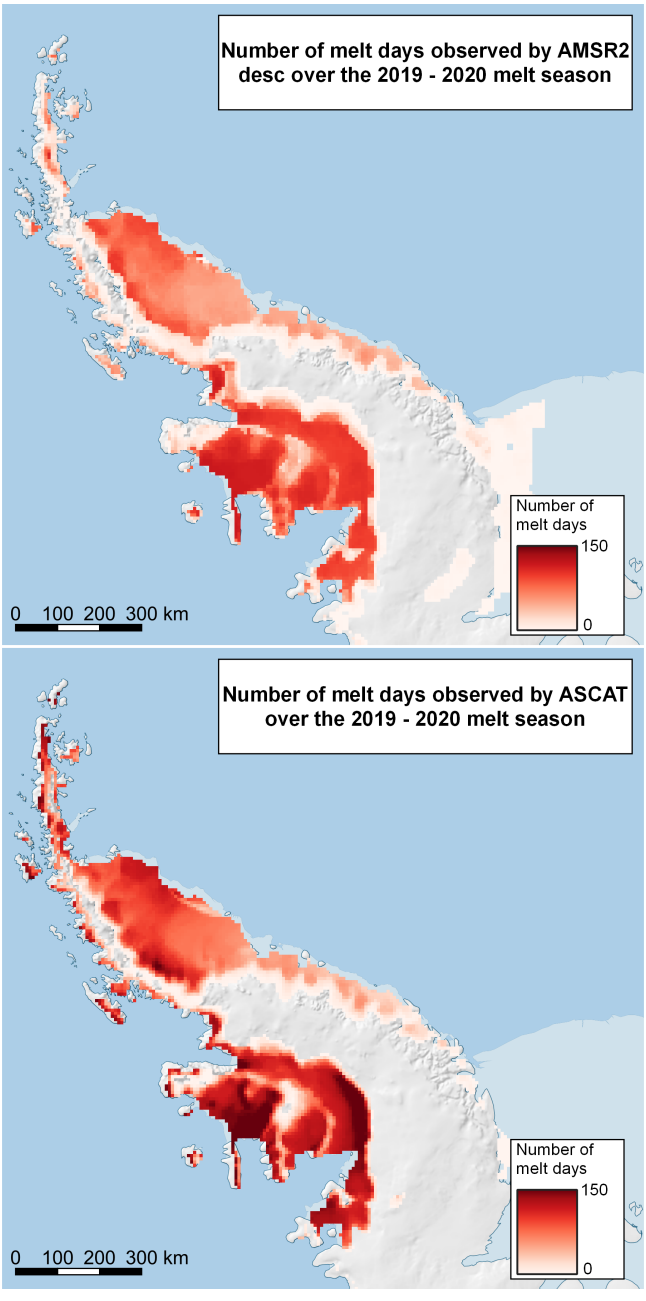

Figure 12. a) Number of melt days observed by AMSR2 on the AP for the 2019-2020 melt season. b) Number of melt days observed by ASCAT on the AP for the 2019-2020 melt season.

in SMB, for the 2019-2020 melt season. Nonetheless, runoff values are relatively small compared to the surface mass balance.

https://doi.org/10.5194/egusphere-2022-1371
Preprint. Discussion started: 15 December 2022

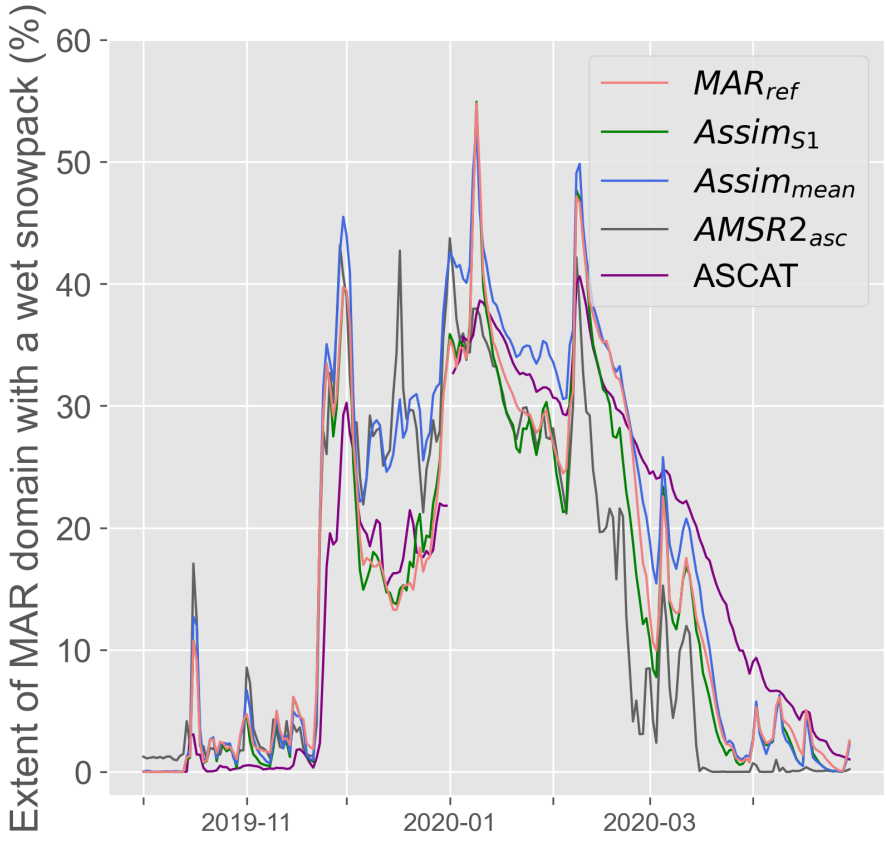

Figure 13. Evolution of the surface melt extent during the 2019-2020 melt season as modeled by MAR_{ref} (in light red), $Assim_{mean}$ (in blue), the assimilation of only S1 melt mask ($Assim_{S1}$, in green), and as observed by AMSR2 in ascending orbit (in grey), and by ASCAT (in purple).

SMB is therefore only slightly affected (-4.5 %). The general tendency of SMB remains positive in the studied zone. Only the ice shelves show negative SMB during periods of intense melting.

The assimilated dataset was also found to influence the results of the model after data assimilation. Each sensor has its particularities and melt masks may differ from each other. Several of these characteristics have been pinpointed previously. The most important ones are the frequency, the revisit time, and the spatial resolution.

The frequency of the sensor impacts the resulting melt production by its difference in liquid water sensitivity and the depth to which the signal penetrates. Because it is difficult to provide accurate surface water depth estimates (Fricker et al., 2021) and because microwave signals can be blocked by the water in the snowpack, the limit at which we stop the assimilation is not always clear. If there is enough water in the top layers, potential liquid water in the deeper layers cannot be observed. In the same way, a thin layer of water can be interpreted as the presence of melt in the snowpack when the underneath layers are dry. The depth threshold Δ_z has been set with different values for the different wavelengths of the sensors but remains constant

https://doi.org/10.5194/egusphere-2022-1371
Preprint. Discussion started: 15 December 2022

no matter the melting state of the snowpack. Introducing a liquid water content/density varying threshold could decrease the melt production after the assimilation. However, field observation of the evolution of the liquid water present in the snowpack profile would be necessary to introduce and validate such an evolution in the assimilation algorithm.

The revisit time of the satellite is influential as the model is particularly resilient to the nudging of the snowpack temperature if the forcing is not performed every day. The assimilation of only Sentinel-1 (revisit time of 6 days, which translates into one image per 2-3 days) is pretty close to the results of the non-assimilated model. Multiple datasets have to be assimilated during the same day for the model to durably change its behavior. The resilience of the model comes from the refreezing of the snowpack during the night and the winter period. When taking into account a few melt seasons, at the beginning of the melt season, the model snowpack is more or less similar to its previous year state.

Assimilating multiple datasets into MAR does not only have advantages. If some missing information is fulfilled by another dataset, it adds another layer of complexity to the algorithm or additional uncertainties linked to the assimilation method used and its thresholds. Datasets may not carry the same information and may not be compatible for all the time steps. Here, none of the datasets is considered to have better melt detection than the other. A possible enhancement of the technique would be to add weight to the masks in case of contradiction between them. Weight could be constructed using the confidence level of the melt detection technique employed, the satellite spatial resolution, the topography gradient inside the satellite pixels interpolated to the MAR grid, or the sensor sensitivity to water.

The results highlight the importance of data assimilation. While the assimilation does not induce a complete change in the behavior of the model as surface melt remains marginal with respect to snowfall, the snowpack properties tend to deviate from the non-assimilated model impacting at the end the snowpack ability to retain future meltwater. Here, satellite data have only been assimilated for two melt seasons over a small area. The study can be conducted for a longer period of time, at a larger scale or over the Greenland ice sheet where surface melt is the main driver of SMB variability (Slater et al., 2021). Further attention should be given to ice shelves as they are the most sensitive region of Antarctica and important to the Antarctic ice sheet stability (Favier and Pattyn, 2015; Paolo et al., 2015; Sun et al., 2020).

Finally, The results obtained in this paper pinpoint the uncertainties of the regional climate model over the AP. The assimilation of remotely sensed data into RCMs is a promising way of reducing the biases and errors inherent to climate models knowing that there is no direct measurement of meltwater content into the snowpack in Antarctica.

Code and data availability. The MAR code used in this study is tagged as v3.12 on https://gitlab.com/Mar-Group/MARv3 (MAR model, 2022). Instructions to download the MAR code are provided on https://www.mar.cnrs.fr (MAR Team, 2022). The MAR outputs used in this study are available upon request by email (tdethinne@uliege.be) Python code and necessary files to perform the assimilation with MAR are available on https://gitlab.uliege.be/tdethinne/assim_mar

https://doi.org/10.5194/egusphere-2022-1371
Preprint. Discussion started: 15 December 2022

Author contributions. TD and XF conceived the study. TD performed the simulations based on a domain of CK. TD led the writing of the manuscript. TD, QG, GP, XF, CK, and AO discussed the results. TD and GP processed the RS data. CK assisted with AWS data comparison. All co-authorsrevised and contributed to the editing of the manuscript.

Competing interests. The authors declare that they have no conflict of interest.

Acknowledgements. ERA5 reanalysis data (Hersbach et al., 2020) are provided by the European Centre for Medium-Range Weather Forecasts, from their website at https://www.ecmwf.int/en/forecasts/datasets/reanalysis-datasets/era5 (last access: 24 October 2022).

Consortium des Équipements de Calcul Intensif (CÉCI), funded by the Fonds de la Recherche Scientifique de Belgique (F.R.S. – FNRS) under grant no. 2.5020.11 and the Tier-1 supercomputer (Nic5) of the Fédération Wallonie Bruxelles infrastructure funded by the Walloon Region under grant agreement no. 1117545.

Background maps have been provided by the Norwegian Polar Institute through the Quantarctica3 project (Matsuoka et al., 2021).

https://doi.org/10.5194/egusphere-2022-1371
Preprint. Discussion started: 15 December 2022

References

Adusumilli, S., Fricker, H. A., Medley, B., Padman, L., and Siegfried, M. R.: Interannual variations in meltwater input to the Southern Ocean from Antarctic ice shelves, Nature Geoscience, 13, 616–620, https://doi.org/10.1038/s41561-020-0616-z, 2020.

Amante, C. and Eakins, B. W.: ETOPO1 arc-minute global relief model : procedures, data sources and analysis. NOAA technical memorandum NESDIS NGDC-24, https://repository.library.noaa.gov/view/noaa/1163, visited on 2022-10-20, 2009.

Amory, C., Kittel, C., Le Toumelin, L., Agosta, C., Delhasse, A., Favier, V., and Fettweis, X.: Performance of MAR (v3.11) in simulating the drifting-snow climate and surface mass balance of Adélie Land, East Antarctica, Geoscientific Model Development, 14, 3487–3510, https://doi.org/10.5194/gmd-14-3487-2021, 2021.

Ashcraft, I. S. and Long, D. G.: Comparison of methods for melt detection over Greenland using active and passive microwave measurements, International Journal of Remote Sensing, 27, 2469–2488, https://doi.org/10.1080/01431160500534465, 2006.

Banwell, A. F., Datta, R. T., Dell, R. L., Moussavi, M., Brucker, L., Picard, G., Shuman, C. A., and Stevens, L. A.: The 32-year record-high surface melt in 2019/2020 on the northern George VI Ice Shelf, Antarctic Peninsula, The Cryosphere, 15, 909–925, https://doi.org/10.5194/tc-15-909-2021, 2021.

Barrand, N. E., Vaughan, D. G., Steiner, N., Tedesco, M., Kuipers Munneke, P., van den Broeke, M. R., and Hosking, J. S.: Trends in Antarctic Peninsula surface melting conditions from observations and regional climate modeling, Journal of Geophysical Research: Earth Surface, 118, 315–330, https://doi.org/10.1029/2012JF002559, 2013.

Bell, R. E., Banwell, A. F., Trusel, L. D., and Kingslake, J.: Antarctic surface hydrology and impacts on ice-sheet mass balance, Nature Climate Change, 8, 1044–1052, https://doi.org/10.1038/s41558-018-0326-3, 2018.

Bouchard, A., Rabier, F., Guidard, V., and Karbou, F.: Enhancements of Satellite Data Assimilation over Antarctica, Monthly Weather Review, 138, 2149 – 2173, https://doi.org/10.1175/2009MWR3071.1, 2010.

Brun, E., David, P., Sudul, M., and Brunot, G.: A numerical model to simulate snow-cover stratigraphy for operational avalanche forecasting, Journal of Glaciology, 38, 13–22, https://doi.org/10.3189/s0022143000009552, 1992.

Church, J., Clark, P., Cazenave, A., Gregory, J., Jevrejeva, S., Levermann, A., Merrifield, M., Milne, G., Nerem, R., Nunn, P., Payne, A., Pfeffer, W., Stammer, D., and Unnikrishnan, A.: Sea Level Change, in: Climate Change 2013: The Physical Science Basis. Contribution of Working Group I to the Fifth Assessment Report of the Intergovernmental Panel on Climate Change, edited by Stocker, T., Qin, D., Plattner, G.-K., Tignor, M., Allen, S., Boschung, J., Nauels, A., Xia, Y., Bex, V., and Midgley, P., Cambridge University Press, Cambridge, United Kingdom and New York, NY, USA., 2013.

Chuter, S. J., Zammit-Mangion, A., Rougier, J., Dawson, G., and Bamber, J. L.: Mass evolution of the Antarctic Peninsula over the last 2 decades from a joint Bayesian inversion, The Cryosphere, 16, 1349–1367, https://doi.org/10.5194/tc-16-1349-2022, 2022.

Colosio, P., Tedesco, M., Ranzi, R., and Fettweis, X.: Surface melting over the Greenland ice sheet derived from enhanced resolution passive microwave brightness temperatures (1979–2019), The Cryosphere, 15, 2623–2646, https://doi.org/10.5194/tc-15-2623-2021, 2021.

Datta, R. T., Tedesco, M., Agosta, C., Fettweis, X., Kuipers Munneke, P., and van den Broeke, M. R.: Melting over the northeast Antarctic Peninsula (1999–2009): evaluation of a high-resolution regional climate model, The Cryosphere, 12, 2901–2922, https://doi.org/10.5194/tc-12-2901-2018, 2018.

Datta, R. T., Tedesco, M., Fettweis, X., Agosta, C., Lhermitte, S., Lenaerts, J. T. M., and Wever, N.: The Effect of Foehn-Induced Surface Melt on Firn Evolution Over the Northeast Antarctic Peninsula, Geophysical Research Letters, 46, 3822–3831, https://doi.org/10.1029/2018GL080845, 2019.

https://doi.org/10.5194/egusphere-2022-1371
Preprint. Discussion started: 15 December 2022

Delhasse, A., Kittel, C., Amory, C., Hofer, S., van As, D., S. Fausto, R., and Fettweis, X.: Brief communication: Evaluation of the near-surface climate in ERA5 over the Greenland Ice Sheet, The Cryosphere, 14, 957–965, https://doi.org/10.5194/tc-14-957-2020, 2020.

Donat-Magnin, M., Jourdain, N. C., Kittel, C., Agosta, C., Amory, C., Gallée, H., Krinner, G., and Chekki, M.: Future surface mass balance and surface melt in the Amundsen sector of the West Antarctic Ice Sheet, The Cryosphere, 15, 571–593, https://doi.org/10.5194/tc-15-571-2021, 2021.

Elachi, C. and van Zyl, J.: Nature and Properties of Electromagnetic Waves, in: Introduction to the Physics and Techniques of Remote Sensing, chap. 2, pp. 23–50, John Wiley and Sons, Ltd, https://doi.org/10.1002/0471783390.ch2, 2006.

ESA: The Sentinel-1 Toolbox, https://sentinel.esa.int/web/sentinel/toolboxes/sentinel-1, visited on 2022-10-19, 2022.

Evensen, G.: Data assimilation: The ensemble kalman filter, Springer Berlin, Heidelberg, https://doi.org/10.1007/978-3-642-03711-5, 2009.

Fahnestock, M. A., Abdalati, W., and Shuman, C. A.: Long melt seasons on ice shelves of the Antarctic Peninsula: an analysis using satellite-based microwave emission measurements, Annals of Glaciology, 34, 127–133, https://doi.org/10.3189/172756402781817798, 2002.

Favier, L. and Pattyn, F.: Antarctic ice rise formation, evolution, and stability, Geophysical Research Letters, 42, 4456–4463, https://doi.org/10.1002/2015GL064195, 2015.

Fettweis, X., Tedesco, M., van den Broeke, M., and Ettema, J.: Melting trends over the Greenland ice sheet (1958–2009) from spaceborne microwave data and regional climate models, The Cryosphere, 5, 359–375, https://doi.org/10.5194/tc-5-359-2011, 2011.

Fettweis, X., Hofer, S., Séférian, R., Amory, C., Delhasse, A., Doutreloup, S., Kittel, C., Lang, C., Van Bever, J., Veillon, F., and Irvine, P.: Brief communication: Reduction in the future Greenland ice sheet surface melt with the help of solar geoengineering, The Cryosphere, 15, 3013–3019, https://doi.org/10.5194/tc-15-3013-2021, 2021.

Fretwell, P., Pritchard, H. D., Vaughan, D. G., Bamber, J. L., Barrand, N. E., Bell, R., Bianchi, C., Bingham, R. G., Blankenship, D. D., Casassa, G., Catania, G., Callens, D., Conway, H., Cook, A. J., Corr, H. F. J., Damaske, D., Damm, V., Ferraccioli, F., Forsberg, R., Fujita, S., Gim, Y., Gogineni, P., Griggs, J. A., Hindmarsh, R. C. A., Holmlund, P., Holt, J. W., Jacobel, R. W., Jenkins, A., Jokat, W., Jordan, T., King, E. C., Kohler, J., Krabill, W., Riger-Kusk, M., Langley, K. A., Leitchenkov, G., Leuschen, C., Luyendyk, B. P., Matsuoka, K., Mouginot, J., Nitsche, F. O., Nogi, Y., Nost, O. A., Popov, S. V., Rignot, E., Rippin, D. M., Rivera, A., Roberts, J., Ross, N., Siegert, M. J., Smith, A. M., Steinhage, D., Studinger, M., Sun, B., Tinto, B. K., Welch, B. C., Wilson, D., Young, D. A., Xiangbin, C., and Zirizzotti, A.: Bedmap2: improved ice bed, surface and thickness datasets for Antarctica, The Cryosphere, 7, 375–393, https://doi.org/10.5194/tc-7-375-2013, 2013.

Fricker, H. A., Arndt, P., Brunt, K. M., Datta, R. T., Fair, Z., Jasinski, M. F., Kingslake, J., Magruder, L. A., Moussavi, M., Pope, A., Spergel, J. J., Stoll, J. D., and Wouters, B.: ICESat-2 Meltwater Depth Estimates: Application to Surface Melt on Amery Ice Shelf, East Antarctica, Geophysical Research Letters, 48, e2020GL090 550, https://doi.org/10.1029/2020GL090550, 2021.

Gallée, H. and Schayes, G.: Development of a Three-Dimensional Meso-γ Primitive Equation Model: Katabatic Winds Simulation in the Area of Terra Nova Bay, Antarctica, Monthly Weather Review, 122, 671 – 685, https://doi.org/10.1175/1520-0493(1994)122<0671:DOATDM>2.0.CO;2, 1994.

GEE: Sentinel-1 Algorithms, https://developers.google.com/earth-engine/guides/sentinel1, visited on 2022-10-19, 2022.

Gilbert, E. and Kittel, C.: Surface Melt and Runoff on Antarctic Ice Shelves at 1.5°C, 2°C, and 4°C of Future Warming, Geophysical Research Letters, 48, 9, https://doi.org/10.1029/2020GL091733, 2021.

Glaude, Q., Amory, C., Berger, S., Derauw, D., Pattyn, F., Barbier, C., and Orban, A.: Empirical Removal of Tides and Inverse Barometer Effect on DInSAR From Double DInSAR and a Regional Climate Model, IEEE Journal of Selected Topics in Applied Earth Observations and Remote Sensing, 13, 4085–4094, https://doi.org/10.1109/JSTARS.2020.3008497, 2020.

https://doi.org/10.5194/egusphere-2022-1371
Preprint. Discussion started: 15 December 2022

Gorelick, N., Hancher, M., Dixon, M., Ilyushchenko, S., Thau, D., and Moore, R.: Google Earth Engine: Planetary-scale geospatial analysis for everyone, Remote Sensing of Environment, 202, 18–27, https://doi.org/10.1016/j.rse.2017.06.031, big Remotely Sensed Data: tools, applications and experiences, 2017.

Hersbach, H., Bell, B., Berrisford, P., Biavati, G., Horányi, A., Muñoz Sabater, J., Nicolas, J., Peubey, C., Radu, R., Rozum, I., Schepers, D., Simmons, A., Soci, C., Dee, D., and Thépaut, J.-N.: ERA5 hourly data on single levels from 1979 to present, https://doi.org/10.24381/cds.adbb2d47, visited on 2022-01-22, 2018.

Hersbach, H., Bell, B., Berrisford, P., Hirahara, S., Horányi, A., Muñoz-Sabater, J., Nicolas, J., Peubey, C., Radu, R., Schepers, D., Simmons, A., Soci, C., Abdalla, S., Abellan, X., Balsamo, G., Bechtold, P., Biavati, G., Bidlot, J., Bonavita, M., De Chiara, G., Dahlgren, P., Dee, D., Diamantakis, M., Dragani, R., Flemming, J., Forbes, R., Fuentes, M., Geer, A., Haimberger, L., Healy, S., Hogan, R. J., Hólm, E., Janisková, M., Keeley, S., Laloyaux, P., Lopez, P., Lupu, C., Radnoti, G., de Rosnay, P., Rozum, I., Vamborg, F., Villaume, S., and Thépaut, J.-N.: The ERA5 global reanalysis, Quarterly Journal of the Royal Meteorological Society, 146, 1999–2049, https://doi.org/10.1002/qj.3803, 2020.

Husman, S. D. R., Zhongyang, H., Wouters, B., Munneke, P. K., Veldhuijsen, S., and Lhermitte, S.: Remote Sensing of Surface Melt on Antarctica: Opportunities and Challenges, Journal of selected topics in applied earth observations and remote sensing, https://doi.org/10.1109/JSTARS.2022.3216953, 2022.

Johnson, A., Fahnestock, M., and Hock, R.: Evaluation of passive microwave melt detection methods on Antarctic Peninsula ice shelves using time series of Sentinel-1 SAR, Remote Sensing of Environment, 250, https://doi.org/10.1016/j.rse.2020.112044, 2020.

Johnson, A., Hock, R., and Fahnestock, M.: Spatial variability and regional trends of Antarctic ice shelf surface melt duration over 1979–2020 derived from passive microwave data, Journal of Glaciology, 68, 533–546, https://doi.org/10.1017/jog.2021.112, 2022.

Kittel, C.: Present and future sensitivity of the Antarctic surface mass balance to oceanic and atmospheric forcings: insights with the regional climate model MAR, Ph.D. thesis, ULiège - Université de Liège, https://hdl.handle.net/2268/258491, 2021.

Kittel, C., Amory, C., Agosta, C., Jourdain, N. C., Hofer, S., Delhasse, A., Doutreloup, S., Huot, P.-V., Lang, C., Fichefet, T., and Fettweis, X.: Diverging future surface mass balance between the Antarctic ice shelves and grounded ice sheet, The Cryosphere, 15, 1215–1236, https://doi.org/10.5194/tc-15-1215-2021, 2021.

Kittel, C., Fettweis, X., Picard, G., and Gourmelen, N.: Assimilation of satellite-derived melt extent increases melt simulated by MAR over the Amundsen sector (West Antarctica), Bulletin de la Société Géographique de Liège, 78, 87–99, https://doi.org/10.25518/0770-7576.6616, 2022.

Koskinen, J., Pulliainen, J., and Hallikainen, M.: The use of ERS-1 SAR data in snow melt monitoring, IEEE Transactions on Geoscience and Remote Sensing, 35, 601–610, https://doi.org/10.1109/36.581975, 1997.

Lai, C.-Y., Kingslake, J., Wearing, M. G., Chen, P.-H. C., Gentine, P., Li, H., Spergel, J. J., and van Wessem, J. M.: Vulnerability of Antarctica's ice shelves to meltwater-driven fracture, Nature, 584, 574–578, https://doi.org/10.1038/s41586-020-2627-8, 2020.

Lambin, C., Fettweis, X., Kittel, C., Fonder, M., and Ernst, D.: Assessment of future wind speed and wind power changes over South Greenland using the Modèle Atmosphérique Régional regional climate model, International Journal of Climatology, pp. 1–17, https://doi.org/10.1002/joc.7795, 2022.

Landmann, J. M., Künsch, H. R., Huss, M., Ogier, C., Kalisch, M., and Farinotti, D.: Assimilating near-real-time mass balance stake readings into a model ensemble using a particle filter, The Cryosphere, 15, 5017–5040, https://doi.org/10.5194/tc-15-5017-2021, 2021.

Liang, D., Guo, H., Zhang, L., Cheng, Y., Zhu, Q., and Liu, X.: Time-series snowmelt detection over the Antarctic using Sentinel-1 SAR images on Google Earth Engine, Remote Sensing of Environment, 256, 112 318, https://doi.org/10.1016/j.rse.2021.112318, 2021.

https://doi.org/10.5194/egusphere-2022-1371
Preprint. Discussion started: 15 December 2022

Lindsley, R. D. and Long, D. G.: Enhanced-Resolution Reconstruction of ASCAT Backscatter Measurements, IEEE Transactions on Geoscience and Remote Sensing, 54, 2589–2601, https://doi.org/10.1109/TGRS.2015.2503762, 2016.

MAR model: http://www.mar.cnrs.fr, visited on 2022-11-10, 2022.

MAR Team: MARv3.12, https://gitlab.com/Mar-Group/, visited on 2022-11-16, 2022.

Matsuoka, K., Skoglund, A., Roth, G., de Pomereu, J., Griffiths, H., Headland, R., Herried, B., Katsumata, K., Le Brocq, A., Licht, K., Morgan, F., Neff, P. D., Ritz, C., Scheinert, M., Tamura, T., Van de Putte, A., van den Broeke, M., von Deschwanden, A., Deschamps-Berger, C., Van Liefferinge, B., Tronstad, S., and Melvær, Y.: Quantarctica, an integrated mapping environment for Antarctica, the Southern Ocean, and sub-Antarctic islands, Environmental Modelling and Software, 140, https://doi.org/10.1016/j.envsoft.2021.105015, 2021.

Morcrette, J.-J.: Assessment of the ECMWF Model Cloudiness and Surface Radiation Fields at the ARM SGP Site, Monthly Weather Review, 130, 257 – 277, https://doi.org/10.1175/1520-0493(2002)130<0257:AOTEMC>2.0.CO;2, 2002.

Moreira, A., Prats-Iraola, P., Younis, M., Krieger, G., Hajnsek, I., and Papathanassiou, K. P.: A tutorial on synthetic aperture radar, IEEE Geoscience and Remote Sensing Magazine, 1, 6–43, https://doi.org/10.1109/MGRS.2013.2248301, 2013.

Mottram, R., Hansen, N., Kittel, C., van Wessem, J. M., Agosta, C., Amory, C., Boberg, F., van de Berg, W. J., Fettweis, X., Gossart, A., van Lipzig, N. P. M., van Meijgaard, E., Orr, A., Phillips, T., Webster, S., Simonsen, S. B., and Souverijns, N.: What is the surface mass balance of Antarctica? An intercomparison of regional climate model estimates, The Cryosphere, 15, 3751–3784, https://doi.org/10.5194/tc-15-3751-2021, 2021.

Mullissa, A., Vollrath, A., Odongo-Braun, C., Slagter, B., Balling, J., Gou, Y., Gorelick, N., and Reiche, J.: Sentinel-1 SAR Backscatter Analysis Ready Data Preparation in Google Earth Engine, Remote Sensing, 13, https://doi.org/10.3390/rs13101954, 2021.

Mätzler, C.: Applications of the interaction of microwaves with the natural snow cover, Remote Sensing Reviews, 2, 259–387, https://doi.org/10.1080/02757258709532086, 1987.

Nagler, T. and Rott, H.: Retrieval of wet snow by means of multitemporal SAR data, IEEE Transactions on Geoscience and Remote Sensing, 38, 754–765, https://doi.org/10.1109/36.842004, 2000.

Nagler, T., Rott, H., Ripper, E., Bippus, G., and Hetzenecker, M.: Advancements for Snowmelt Monitoring by Means of Sentinel-1 SAR, Remote Sensing, 8, https://doi.org/10.3390/rs8040348, 2016.

Navari, M., Margulis, S. A., Tedesco, M., Fettweis, X., and Alexander, P. M.: Improving Greenland Surface Mass Balance Estimates Through the Assimilation of MODIS Albedo: A Case Study Along the K-Transect, Geophysical Research Letters, 45, 6549–6556, https://doi.org/10.1029/2018GL078448, 2018.

Noël, B., van de Berg, W. J., Lhermitte, S., Wouters, B., Machguth, H., Howat, I., Citterio, M., Moholdt, G., Lenaerts, J. T. M., and van den Broeke, M. R.: A tipping point in refreezing accelerates mass loss of Greenland's glaciers and ice caps, Nature Communications, 8, 14 730, https://doi.org/10.1038/ncomms14730, 2017.

Paolo, F. S., Fricker, H. A., and Padman, L.: Volume loss from Antarctic ice shelves is accelerating, Science, 348, 327–331, https://doi.org/10.1126/science.aaa0940, 2015.

Parkinson, C.: Satellite Passive Microwave Measurements of Sea Ice, in: Encyclopedia of Ocean Sciences, edited by Steele, J. H., pp. 2531–2539, Academic Press, Oxford, https://doi.org/10.1006/rwos.2001.0336, 2001.

Picard, G. and Fily, M.: Surface melting observations in Antarctica by microwave radiometers: Correcting 26-year time series from changes in acquisition hours, Remote Sensing of Environment, 104, 325–336, https://doi.org/10.1016/j.rse.2006.05.010, 2006.

Picard, G., Leduc-Leballeur, M., Banwell, A. F., Brucker, L., and Macelloni, G.: The sensitivity of satellite microwave observations to liquid water in the Antarctic snowpack, The Cryosphere Discussions, 2022, 1–34, https://doi.org/10.5194/tc-2022-85, 2022.

https://doi.org/10.5194/egusphere-2022-1371
Preprint. Discussion started: 15 December 2022

Pollard, D., DeConto, R. M., and Alley, R. B.: Potential Antarctic Ice Sheet retreat driven by hydrofracturing and ice cliff failure, Earth and Planetary Science Letters, 412, 112–121, https://doi.org/10.1016/j.epsl.2014.12.035, 2015.

Ridder, K. D. and Gallée, H.: Land Surface–Induced Regional Climate Change in Southern Israel, Journal of Applied Meteorology, 37, 1470 – 1485, https://doi.org/10.1175/1520-0450(1998)037<1470:LSIRCC>2.0.CO;2, 1998.

Rignot, E., Mouginot, J., Scheuchl, B., van den Broeke, M., van Wessem, M. J., and Morlighem, M.: Four decades of Antarctic Ice Sheet mass balance from 1979–2017, Proceedings of the National Academy of Sciences, 116, 1095–1103, https://doi.org/10.1073/pnas.1812883116, 2019.

Scambos, T., Hulbe, C., and Fahnestock, M.: Climate-Induced Ice Shelf Disintegration in the Antarctic Peninsula, in: Antarctic Peninsula Climate Variability: Historical and Paleoenvironmental Perspectives, pp. 79–92, American Geophysical Union, https://doi.org/10.1029/AR079p0079, 2003.

Slater, T., Shepherd, A., McMillan, M., Leeson, A., Gilbert, L., Muir, A., Munneke, P. K., Noël, B., Fettweis, X., van den Broeke, M., and Briggs, K.: Increased variability in Greenland Ice Sheet runoff from satellite observations, Nature Communications, 12, 6069, https://doi.org/10.1038/s41467-021-26229-4, 2021.

Sun, S., Pattyn, F., Simon, E. G., Albrecht, T., Cornford, S., Calov, R., Dumas, C., Gillet-Chaulet, F., Goelzer, H., Golledge, N. R., and et al.: Antarctic ice sheet response to sudden and sustained ice-shelf collapse (ABUMIP), Journal of Glaciology, 66, 891–904, https://doi.org/10.1017/jog.2020.67, 2020.

Tedesco, M., Abdalati, W., and Zwally, H. J.: Persistent surface snowmelt over Antarctica (1987–2006) from 19.35 GHz brightness temperatures, Geophysical Research Letters, 34, 1–6, https://doi.org/10.1029/2007GL031199, 2007.

The IMBIE Team: Mass balance of the Antarctic Ice Sheet from 1992 to 2017, Nature, 558, 219–222, https://doi.org/10.1038/s41586-018-0179-y, 2018.

Torinesi, O., Fily, M., and Genthon, C.: Variability and Trends of the Summer Melt Period of Antarctic Ice Margins since 1980 from Microwave Sensors, Journal of Climate, 16, 1047 – 1060, https://doi.org/10.1175/1520-0442(2003)016<1047:VATOTS>2.0.CO;2, 2003.

Trusel, L. D., Frey, K. E., Das, S. B., Munneke, P. K., and van den Broeke, M. R.: Satellite-based estimates of Antarctic surface meltwater fluxes, Geophysical Research Letters, 40, 6148–6153, https://doi.org/10.1002/2013GL058138, 2013.

Trusel, L. D., Frey, K. E., Das, S. B., Karnauskas, K. B., Munneke, P. K., Meijgaard, E. V., and Broeke, M. R. V. D.: Divergent trajectories of Antarctic surface melt under two twenty-first-century climate scenarios, Nature Geoscience, 8, 927–932, https://doi.org/10.1038/ngeo2563, 2015.

Wille, J. D., Favier, V., Jourdain, N. C., Kittel, C., Turton, J. V., Agosta, C., Gorodetskaya, I. V., Picard, G., Codron, F., Santos, C. L.-D., Amory, C., Fettweis, X., Blanchet, J., Jomelli, V., and Berchet, A.: Intense atmospheric rivers can weaken ice shelf stability at the Antarctic Peninsula, Communications Earth & Environment, 3, 90, https://doi.org/10.1038/s43247-022-00422-9, 2022.

Winebrenner, D. P., Nelson, E. D., Colony, R., and West, R. D.: Observation of melt onset on multiyear Arctic sea ice using the ERS 1 synthetic aperture radar, Journal of Geophysical Research: Oceans, 99, 22 425–22 441, https://doi.org/10.1029/94JC01268, 1994.

Zwally, H. J. and Fiegles, S.: Extent and duration of Antarctic surface melting, Journal of Glaciology, 40, 463–475, https://doi.org/10.3189/s0022143000012338, 1994.